Hopf Bifurcation Analysis for a Variant of the Logistic Equation with Delays

Iustina Chifan

Thesis submitted to the Faculty of Science in partial fulfillment of the requirements
for the degree of
Master of Science Mathematics and Statistics[1]

Department of Mathematics and Statistics
Faculty of Science
University of Ottawa

[1]The M.Sc. program is a joint program with Carleton University, administered by the Ottawa-Carleton Institute of Mathematics and Statistics

Abstract

This thesis contains some results on the behavior of a delay differential equation (DDE) with two delays, at a Hopf bifurcation, for the nonzero equilibrium, using the growth rate, r, as bifurcation parameter. This DDE is a model for population growth, incorporating a maturation delay, and a second delay in the harvesting term. Considering a Taylor expansion of the non-dimensionalized model, we find a region of stability for the nonzero equilibrium, after which we find a pair of ODEs which help define the flow on the center manifold. We then find an expression for the first Lypapunov coefficient, which changes sign, so we also find the second Lyapunov coefficient, allowing us to predict multi-stability in the model. Numerical simulations provide examples of the behavior expected. For a similar model with one delay (PMC model), we prove the Hopf bifurcation at the nonzero equilibrium is always supercritical.

Dedications

To my family for all their support.

Acknowledgement

I would like to thank my supervisor Dr. Victor LeBlanc for his excellent guidance, and also the University of Ottawa for their financial support.

Contents

List of Figures

List of Tables

Chapter 1

Introduction

Early mathematical models for the population of a single species, proposed by Euler and later in 1798 by Malthus showed exponential growth of the population, but such an exponential population growth did not seem realistic over a long period of time because of limited resources in the environment [17]. In 1836 Verhulst proposed a population model, equation (1.0.1) below, which is self-limiting, displaying logistic growth:

$$\frac{dN}{dT} = rN(1 - \frac{N}{K}), \tag{1.0.1}$$

where $N(T)$ is the population of a species at time $T, r > 0$ is the intrinsic growth rate, and $K > 0$ is the carrying capacity which would be determined by available resources [16, 17].

Since then, many authors have used techniques from differential equations to study population growth. Among them, in 1978, authors Perez, Malta and Coutinho proposed a slightly modified version of an earlier equation by Maynard Smith in 1968, created to describe phenomenon observed in caged fly populations [19]. An advantage to their model, the Perez-Malta-Coutinho (PMC) equation, is considered to be the use of parameters which are more easily measurable, and have a clearer physical interpretation [16, 19]. This PMC equation was further studied by authors Manjunath, Podapati and Raina in 2017, under the form below [16]:

$$\dot{x}(t) = rx(t - \tau)(c_1 - c_2x(t - \tau)) - \gamma x(t), \tag{1.0.2}$$

where $x(t) > 0$ represents the adult fly population at a particular moment in time t [16]. The time period it takes for an egg to become an adult fly is represented in the model, by use of the time delay $\tau > 0$ [19]. The parameter $r > 0$ represents the intrinsic growth rate, and the terms c_1–$c_2x(t - \tau)$ and γ represent birth rate per head and death rate per head, respectively [16]. It is assumed $c_1, c_2 > 0$ and $\gamma \geq 0$ [16].

This equation is a variant of the logistic equation (1.0.1), used to model population dynamics [16].

This thesis will mainly focus on a slightly modified version of equation (1.0.2). It is considered fitting to add a second delay term, $\tau_2 > 0$ in the death rate term. There are different situations where a delay in the death rate could help make the model more realistic. The death rate per head can be affected by harvesting. One example that includes a delay in the harvesting term, as is mentioned in [12] for fisheries, but here generalizing to any species, is that in a population of plants or animals, some individuals are more desirable to be harvested, so the requirement that animals or plants reach a certain size or age before they can be harvested, adds a delay, τ_2, in the harvesting term. A second situation is that if γ is a harvesting constant, it would be based off the population size at some previous time, and not on the population size at that instant, which would be unknown. In both of these examples, this second delay τ_2 would be in general different from the first delay, τ_1. Thus the modified PMC that we will study is

$$\dot{x}(t) = rx(t-\tau_1)(c_1 - c_2x(t-\tau_1)) - \gamma x(t-\tau_2) \tag{1.0.3}$$

and has the same parameters as (1.0.2) above. Since equations (1.0.2) and (1.0.3) are variants of the logistic equation, their applicability is not restricted to fly populations. Therefore, $x(t)$ will be generalized to represent any population, and τ_1 in (1.0.3) or τ in (1.0.2) will represent the time period required for individuals of the species to reach adulthood, and τ_2 the time delay in harvesting. Most of this thesis will consist of a mathematical analysis of the class of DDEs of the form (1.0.3).

1.0.1 Literature Review

Many authors have studied models incorporating delay differential equations in the context of population dynamics. A common use is to model the population of a single species, incorporating one, two or more delays. Aiello and Freedman studied stability of equilibria for such a model, incorporating stage structure and a delay term [1]. Brauer studied a general model for the population size of a single species that is harvested at a constant rate, with one delay, of the form below:

$$x'(t) = x(t)f(x(t-T)) - H, \tag{1.0.4}$$

giving conditions for the equilibrium to be stable when $H = 0$ and $H > 0$, and criteria the delay term T must satisfy so that the equilibrium of (1.0.4) is asymptotically stable [4]. Braddock and Van Den Driessche analysed a population model using two delays, in the form below:

$$\dot{\eta}(\tau) = -(1+\eta(\tau))[f\eta(\tau-1) + g\eta(\tau-\theta)] \text{ where } \theta = \frac{T_2}{T_1} \geq 1 \tag{1.0.5}$$

(where T_1 and T_2 are the delays), finding regions of linear stability for the case when $f = g$, for general f and g under certain conditions, as well as generalizing some results to models with more delays [3].

In a more general context, Li et al. studied a delay differential equation with two delays, looking at the stability of the zero solution, and determining conditions under which the equation undergoes a Hopf bifurcation, and deriving formulas to determine its properties [15]. This thesis will use some of the results from this paper to determine a region of stability for the nonzero equilibrium.

In nature, many species live together and interact in an ecosystem, so it is natural that the populations of these species affect each other. So to get a better idea of population dynamics it could be of use to study the population not only of a species, but by studying models that include interactions with other species, a common example being the predator prey interaction.

Although not the specific focus of this thesis, we mention that many authors have studied such population models. Many authors have looked at different types of predator-prey systems with a single delay, studying equilibrium stability and properties of the Hopf bifurcation, like in [2, 5, 25]. Some differences in those predator-prey models include considering a disease in the predator species [25], a carrying capacity which is proportional to prey density [5], and a system which takes into account habitat complexity, thought to affect the predator's chances of capturing prey, and includes a gestation delay [2]. Song et al. analysed such a model, incorporating *stage structure* (population is split between immature and mature) and a time delay for the prey, studying equilibrium stability and existence of a Hopf bifurcation [23]. Similar studies have also been done for such systems incorporating two delays, like in [18, 21]. Senthilkumaran and Gunasundari consider such a model with stage structure for the predator population, a gestation delay for the prey, a second delay for predator maturation, to take into account the delay that occurs between when a predator consumes prey and reproduces, and considering a logistic growth for the prey population [21]. Peng et al. consider a controlled predator prey system (to delay the appearance of a Hopf bifurcation), with τ_1 being a gestation time delay for predator and prey and τ_2 to take into account predator maturation, which affects their hunting of prey, and contribution to the species growth [18].

Brauer also looked at a predator-prey model with a delay and harvesting of the prey species, giving conditions for the equilibrium to be asymptotically stable, as well as bounds on the delay that give a stable system [4]. In comparing this model with the single species model, Brauer found that the one species model could sustain a higher harvesting rate, and among the particular models used as examples, found that harvesting will tend to stabilize the one species model, but have the opposite effect on the predator-prey one, and for a large enough harvesting rate, the single species model could be stable for a longer delay [4].

Another example is the case of two interacting species where both species help

limit the population growth of the other, like the Lotka-Volterra competition system considered by Song et al., which incorporated two delays [22]. Here, the authors studied the stability of the equilibrium, conditions under which the system undergoes a Hopf bifurcation and derived formulas to determine properties of the Hopf bifurcation [22].

The properties of the Hopf bifurcation have been studied in [2, 5, 8, 15, 16, 18, 21, 22, 25], where the authors have used the normal form theory and the center manifold theorem introduced by Hassard, Kazarinoff and Wan in 1981 [10], for ordinary differential equations (ODEs), to derive formulas allowing them to determine the direction of the Hopf bifurcation and the stability and period of the bifurcating periodic solutions. This thesis however, will use a different method, developed by Faria and Magalhães [7], for delay differential equations, to determine the first Lyapunov coefficient, and to study the stability of the Hopf bifurcation. The advantage of this method is that it involves fewer computations and the formula given for finding the first Lyapunov coefficient involves coefficients from the original equation [7].

Many authors analysed models which considered a gestation or maturation delay, among which [1, 2, 8, 13, 18, 21, 23]. Others have also looked at models where the harvesting term has a delay. For example, Kar looked at the stability of the equilibrium for two prey-predator models, with one model including a time delay in the harvesting term for the predator species, and the other for the prey species [12]. In these models, the time delay is included to take into account a selective harvesting, done on the basis of age and size of the individual [12].

Delay differential equations have also been studied in epidemiology. For example, they have been used by authors to develop a model to study the spread of a bacterial infection in a mosquito population [26]. A second example is a generalized susceptible-infected-susceptible model, with a delay, used to model the spread of a disease in a human population, through a vector agent, like mosquitos, where the authors study the stability of the equilibria [11].

In conclusion, DDEs are an important modelling tool for population dynamics and so it is important to understand their dynamic behavior at bifurcations.

1.0.2 Examples

Two simple examples below will illustrate two aspects related to equations (1.0.2) and (1.0.3). The first example will show the process of finding equilibrium points, and determining their stability for the logistic equation, and the second example will show how adding a delay term to a simple ODE complicates the dynamics of the solutions.

Example 1 As equations (1.0.2) and (1.0.3) defined in the introduction are variants of the logistic equation, this example will look at the behavior of solutions to the logistic equation (1.0.1). Setting the right hand side of (1.0.1) equal to zero, and

solving for N gives two equilibrium points, $N^* = 0$ and $N^* = K$. To determine the behaviour of the solutions, the derivative of the right hand side of (1.0.1), which will be called $f'(N)$, where

$$f'(N) = r - \frac{2r}{K}N, \tag{1.0.6}$$

is evaluated at both equilibrium points. This shows

$$f'(0) = r > 0 \tag{1.0.7}$$
$$f'(K) = -r < 0, \tag{1.0.8}$$

so $N^* = 0$ is unstable and $N^* = K$ is stable.

Figure 1.1: Phase Diagram for the Logistic Equation.

The corresponding phase diagram, shown in Figure 1.1, shows that solutions of the logistic equation converge to K, the carrying capacity. If the population starts below K (but above 0), it will grow to the carrying capacity, and if the population starts off higher than the carrying capacity, it will decrease to the carrying capacity.

Example 2 Now, it will be shown, with the use of a simple ordinary differential equation (ODE), how the addition of a single delay leads to more complicated dynamics. Starting with the initial value problem (IVP) below:

$$\dot{x}(t) = ax(t) \text{ with initial condition } x(0) = x_0. \tag{1.0.9}$$

The above IVP is simple to solve. It results in the characteristic equation $\lambda - a = 0$, which gives one eigenvalue $\lambda = a$, giving a general solution of $x(t) = c_1 e^{at}$. Further, using the initial condition which implies $c_1 = x_0$, gives the unique solution

$$x(t) = x_0 e^{at}. \tag{1.0.10}$$

Now, including a delay term in the above equation (1.0.9) gives the following delay differential equation (DDE):

$$\dot{x}(t) = ax(t-1). \tag{1.0.11}$$

To find solutions to the above equation the characteristic equation is needed. To find the characteristic equation the ansatz $e^{\lambda t}$ is substituted into (1.0.11), giving

$$\lambda e^{\lambda t} = ae^{\lambda(t-1)}, \tag{1.0.12}$$

and simplifying gives

$$\lambda = ae^{-\lambda}, \tag{1.0.13}$$

which is clearly a much more complicated characteristic equation than for the ODE above which gave one eigenvalue resulting in the only solution. The characteristic equation of the DDE has infinitely many solutions in $\mathbb{C}$. For example, if we set $\lambda = \beta + i\omega$, (1.0.13) becomes

$$\beta + i\omega = ae^{-\beta - i\omega} = ae^{-\beta}\cos(\omega) - iae^{-\beta}\sin(\omega), \tag{1.0.14}$$

and now splitting real and imaginary parts gives

$$\begin{aligned} \beta &= ae^{-\beta}\cos(\omega) \\ \text{and} \quad \omega &= -ae^{-\beta}\sin(\omega). \end{aligned} \tag{1.0.15}$$

Squaring both sides of the equations in (1.0.15), and adding gives

$$\omega = \pm\sqrt{a^2e^{-2\beta} - \beta^2} \quad + 2\pi n \text{ where } n \in \mathbb{Z}, \tag{1.0.16}$$

so, there are infinitely many choices for ω.

1.0.3 Overview of the Thesis

In a previous section, we mentioned some authors that have studied topics that will be the focus of this thesis: equilibrium stability and properties of the Hopf bifurcation, for DDEs modeling a species population. With *Example 2* above, we gave a small example of how studying the behavior of a DDE is more complicated than for an ODE.

A Hopf bifurcation in a differential equation occurs when a parameter crosses a critical value, and results in the loss of stability at the equilibrium through periodic oscillations, resulting either from the appearance of a stable limit cycle, or the disappearance of an unstable limit cycle [14]. This type of bifurcation can happen in a system which contains a pair of purely imaginary eigenvalues and all other eigenvalues have a real part which is nonzero, and can be examined by varying a parameter (in the case of multiple parameters, all but one are fixed) [24]. Many authors use the delay as bifurcation parameter for example [5, 25] or one of the delays as in [15]. In

this thesis, the growth rate r will be used as bifurcation parameter to investigate the Hopf bifurcation. Since equations (1.0.2) and (1.0.3) above are modeling the population of a species, it would be of interest to know if a Hopf bifurcation occurs, as that would imply oscillations in the population level, which could potentially lead to population extinction unexpectedly and under certain conditions can make population levels harder to predict. Adding a delay in the harvesting term helps make the model more realistic, for reasons previously mentioned. Since many species are endangered, some because of overhunting or overfishing, it would be important to study how harvesting affects population level, to get a better idea of when a species is in danger of extinction.

We start with a short summary on studying the behavior of solutions for the simpler case of ODEs, summarizing information from [20, 24] in this paragraph. When considering a system $\dot{x} = f(x)$ with an equilibrium at x_0, if all the eigenvalues associated with the linearization $Df(x_0)$ have a nonzero real part, the linear part of the system is studied to gain information about the system near the equilibrium point of interest, x_0. Then, we know that the solutions are either in the stable manifold, and converge to x_0 as $t \to \infty$ or in the unstable manifold, and solutions converge to x_0 as $t \to -\infty$. However, determining the behavior of solutions at a Hopf bifurcation is more complicated because the system contains a pair of purely imaginary eigenvalues, $\lambda = \pm i\omega$. In this case, to determine the behavior of solutions in the nonlinear system near x_0 we restrict the nonlinear system to the center manifold to study the dynamics near x_0. After obtaining the flow on the center manifold, to help in studying the behavior of this system, we can use normal form theory to simplify the nonlinear part of the system.

For DDEs a similar procedure is applied. As mentioned in a previous section, in order to study the Hopf bifurcation we use the method from Faria and Magalhães, referring to both [6] and [7] to summarize the procedure in this paragraph, unless another source is cited. DDEs are infinite-dimensional, as can be seen from the initial condition which is defined on an interval of t-values, as opposed to ODEs for which the initial condition is taken at a certain point, $t = t_0$, and so is finite dimensional [9]. So, for DDEs, we consider the infinite dimensional DDE as an abstract ODE in an infinite dimensional phase space. Then, to obtain the center manifold, the solutions from the infinite dimensional space are projected onto a finite dimensional invariant space associated with the solutions to the characteristic equation (where solutions have $Re(\lambda) = 0$) for the DDE linearized at the equilibrium under study. In this way we obtain ODEs which describe the flow on the center manifold, for which we find the normal form. From [7], we know that the normal form on the center manifold at a Hopf bifurcation, in polar coordinates, $\rho e^{i\zeta}$, truncating the higher order terms, is a system of the form

$$\dot{\rho} = r\lambda'(0)\rho + K\rho^3 + K_4\rho^5 \tag{1.0.17a}$$

$$\dot{\zeta} = -\omega, \tag{1.0.17b}$$

where r is the bifurcation parameter and $\lambda'(0)$ (which is explained in Chater 3) is assumed positive. In these coordinates, periodic solutions correspond to roots of the $\dot{\rho}$ equation in (1.0.17a). In studying the Hopf bifurcation we first focus on computing K. This nonlinear coefficient, K, in front of the cubic term is called the *first Lyapunov coefficient* and is used to determine the type of Hopf bifurcation [14]. In [7] authors Faria and Magalhães give a formula for computing K in terms of the coefficients from the original DDE.

As long as $K \neq 0$, there are two types of Hopf bifurcation possible, supercritical and subcritical. When $K < 0$, the Hopf bifurcation is supercritical (Figure 1.2) and the system goes from having a single, stable equilibrium, which looses stability after the parameter increases past a critical value, and results in the appearance of a stable limit cycle [14]. If $K > 0$, the bifurcation is subcritical (Figure 1.3), and the system goes from having an unstable limit cycle which disappears as the parameter increases past a critical value, at which point the equilibrium stability also changes, from stable to unstable [14]. Considering a parameter r, for which a Hopf bifurcation occurs at a critical value, r_0, we have two plots of the amplitude, by r, to show the behavior of a supercritical compared to a subcritical bifurcation.

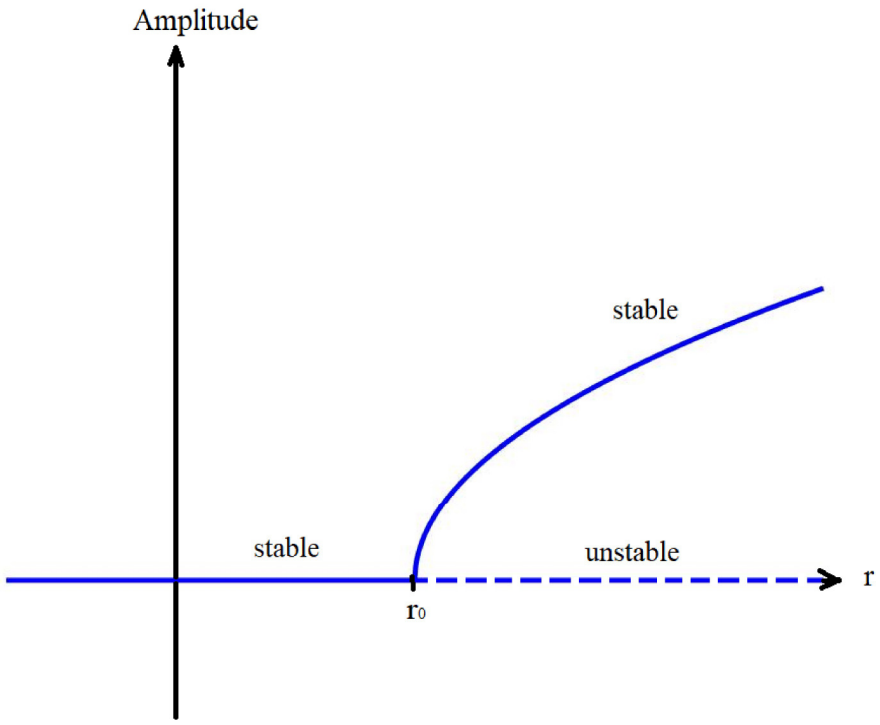

Figure 1.2: Supercritical Hopf bifurcation ($K < 0$).

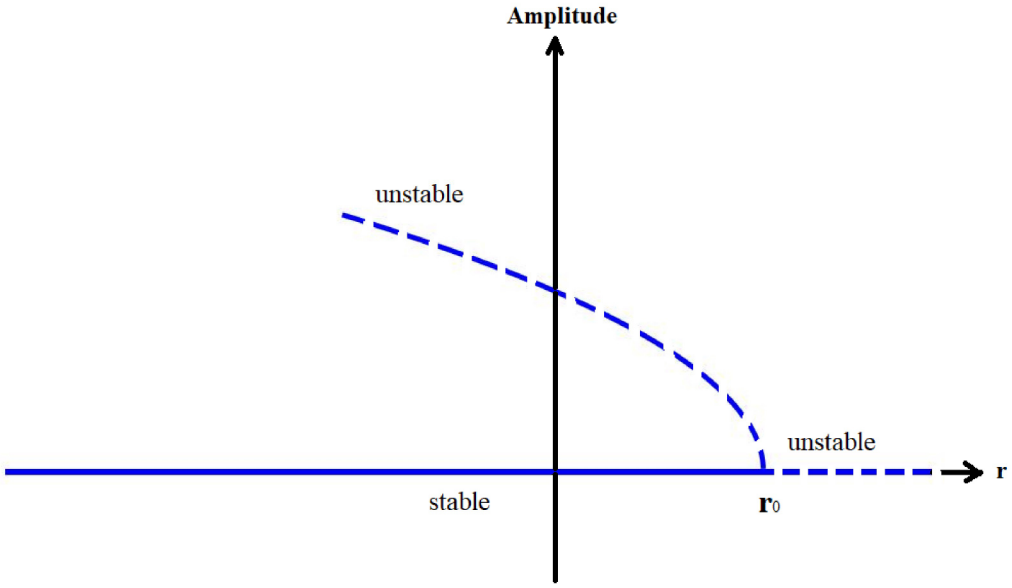

Figure 1.3: Subcritical Hopf bifurcation ($K > 0$).

If $K \approx 0$, the bifurcation is called a *Bautin Bifurcation* and we need to compute K_4, the nonlinear coefficient of ρ^5, which corresponds to the *second Lyapunov coefficient* [7, 14]. Depending on the relative signs of K and K_4, the Hopf bifurcation can turn from supercritical to subcritical, or subcritical to supercritical [14].

For a Hopf bifurcation to turn from supercritical to subcritical, the first Lyapunov coefficient is negative while the second is positive, a behavior which is shown in Figure 1.4 in a plot of amplitude by r. From Figure 1.4, we see that when $r < r_0$, we have a stable equilibrium and an unstable limit cycle, so that solutions within the limit cycle will converge to the equilibrium, while those starting outside the limit cycle will not converge. For r between r_0 and r_1, we have an unstable equilibrium, and two limit cycles, a stable limit cycle inside an unstable limit cycle. When r is within this interval, solutions starting within the unstable limit cycle will converge to the stable limit cycle, while solutions starting outside of this outer limit cycle will not converge. For $r > r_1$, we are left with an unstable equilibrium, and so the solutions will not converge.

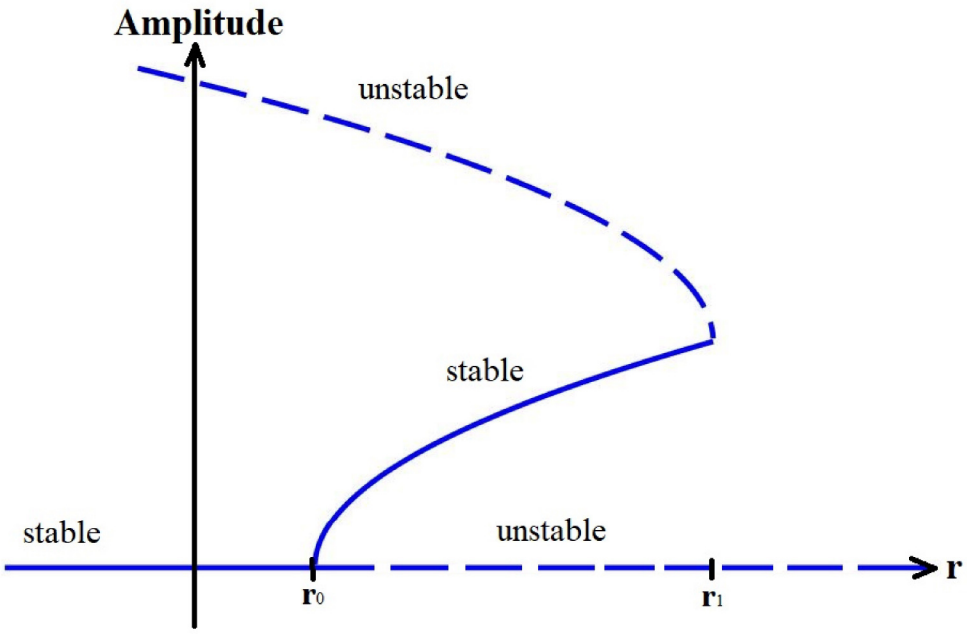

Figure 1.4: Behavior at the Bautin bifurcation, where the Hopf bifurcation turns from supercritical to subcritical.

When the first Lyapunov coefficient is positive and the second Lyapunov coefficient is negative is when the Hopf bifurcation turns from subcritical to supercritical, as shown in Figure 1.5. From Figure 1.5, it can be seen that when $r < r_1$, we have a stable equilibrium. For r between r_1 and r_0, we see *multi-stability*, so that the behavior observed in the solutions depends on the initial condition. We have a stable equilibrium, and two limit cycles, an unstable limit cycle inside a stable limit cycle. When r is within this interval, solutions starting inside the unstable limit cycle will tend to the equilibrium, while solutions starting outside of the inner, unstable limit cycle will converge to the stable, outer, limit cycle. For $r > r_0$, the inner limit cycle disappears, via a subcritical Hopf bifurcation, while the equilibrium looses stability, so now all solutions converge to the limit cycle. One of our main new results in this thesis will be to show that this type of Bautin bifurcation can occur in equation (1.0.3). Consequently, the presence of multi-stability can make it harder to predict the population level. This is because in order to predict the population level, for a growth rate between r_1 and r_0, one would need to know the initial condition, and even then, a small difference in initial condition could make the difference between equilibrium or oscillating population levels as a limiting state.

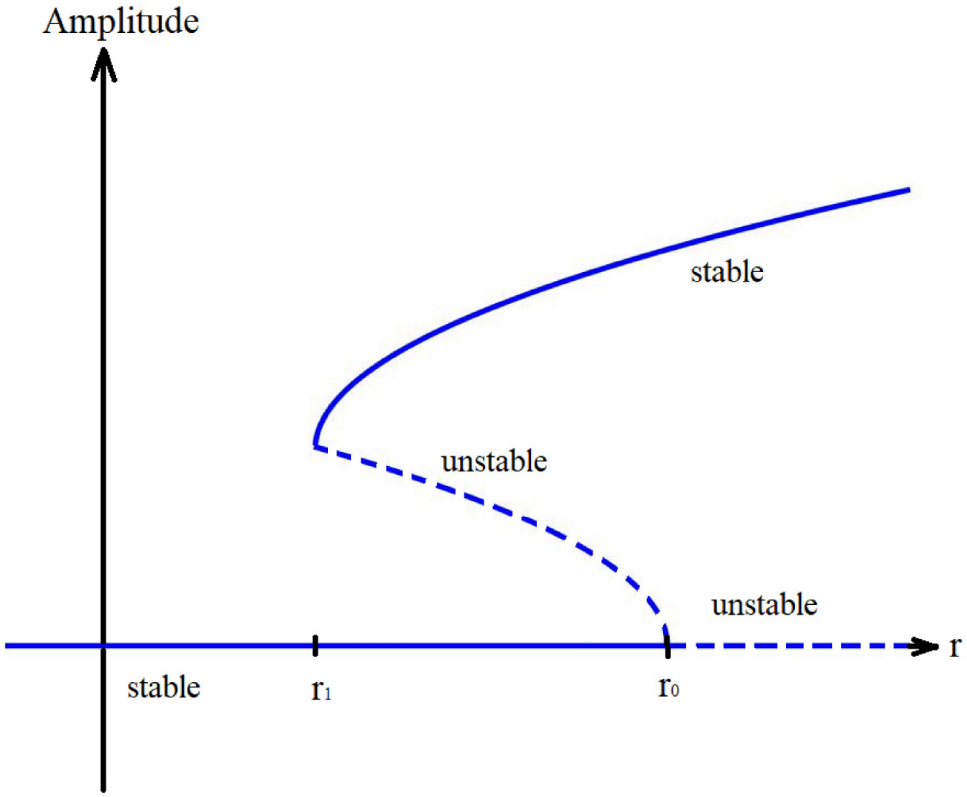

Figure 1.5: Behavior at the Bautin bifurcation, where the Hopf bifurcation turns from subcritical to supercritical.

If the first and second Lyapunov coefficients are both negative, or positive, we expect a behavior similar to that shown in Figure 1.2 and 1.3, respectively, since the Hopf bifurcation is not expected to turn, so we do not expect a second limit cycle.

The chapters of this thesis are organized as follows. In Chapter 2 we find the equilibrium points and focus on the stability of the positive equilibrium of equation (1.0.3). Chapter 3 focuses on finding ODEs on the center manifold for equation (1.0.3). In Chapter 4, we study the PMC model, for which we are expanding on the work done in [16], where the authors do not explicity write down a formula for the first Lyapunov coefficient, K, only saying that it is lengthy and then evaluate it numerically for specific parameter values. So, we find an expression for the first Lyapunov coefficient, and prove that this K is always ≤ 0, $\forall\omega$, giving one of the new results in this thesis. In Chapter 5, we find the first Lyapunov coefficient, K, for (1.0.3), and obtain a plot of K by ω, showing that it is possible for K to change sign, and so brings about the need to compute the second Lyapunov coefficient in the associated Bautin bifurcation, which is done in Chapter 6. Finally, Chapter 7 contains some numerical simulations for both models, created using the program R.

The results of these numerical simulations will confirm the predictions made from our mathematical analysis. The numerical simulations included for the PMC model in [16] were phase portraits, some bifurcations diagrams for their non-dimensional bifurcation parameter η, using different values of γ, and a plot of population level by time, focusing on the existence of chaos. The numerical simulations for the PMC model shown in this thesis are different. The results relating to (1.0.3) are all new results. The program Maple was used for the symbolic computations for Chapters 2, 4, 5, and 6. The code for Maple and R can be found in Appendix A and B, respectively, and was written by the author, except for the Maple code that gives a formula for the second Lyapunov coefficient, which was written by my supervisor.

Chapter 2

Stability and Hopf Bifurcation

This chapter will focus on the stability of the positive equilibrium point and existence of a Hopf bifurcation for equation (1.0.3). A region of stability is determined in terms of the parameter r, the growth rate, as that will be the parameter used in a later chapter in studying the Hopf bifurcation.

To do so, the first step will be to non-dimensionalize the model to decrease the number of parameters. Starting from equation (1.0.3) and letting $y(t) = \frac{1}{\tau_1 c_1} x(t)$ and $t = \tau_1 s$, gives the following non-dimensionalized model:

$$\dot{y}(s) = ry(s-1)\left(1 - cy(s-1)\right) - \tilde{\gamma} y(s-\tau), \tag{2.0.1}$$

where $c = \frac{c_2}{c_1}$, $\tilde{\gamma} = \frac{\gamma}{c_1}$ and $\tau = \frac{\tau_2}{\tau_1}$.
So, in the original model (1.0.3), replace:

$$c_1 = 1, c_2 = c, \tilde{\gamma} = \frac{\gamma}{c_1} = \gamma, \tau_1 = 1, \text{and } \tau_2 = \tau \tag{2.0.2}$$

for the non-dimensionalized model.

The next step is to find the equilibrium points of equation (2.0.1), so equation (2.0.1) will be set equal to zero, and the delay terms are ignored because the delay does not effect the equilibrium, since equilibria are constant in time. This will give

$$ry(s)(1 - cy(s)) - \tilde{\gamma} y(s) = 0, \tag{2.0.3}$$

and solving for $y(s)$:

$$y(s)(r(1 - cy(s)) - \tilde{\gamma}) = 0 \tag{2.0.4}$$

gives two equilibrium points, $y_1^* = 0$ and $y_2^* = \frac{r - \tilde{\gamma}}{rc}$. These are the same equilibrium points as for the PMC model [16], with the substitutions described in (2.0.2). This thesis will focus on behavior of the model at the nonzero equilibrium, since the zero

equilibrium corresponds to extinction, so behaviour at the nonzero equilibrium is more interesting.

A quick analysis of stability for (2.0.1) without delay terms, so considering equation (2.0.3), where we let $f(y) = ry(s)(1 - cy(s)) - \tilde{\gamma}y(s)$, shows that since

$$f'(y) = r - 2rcy(s) - \tilde{\gamma}, \tag{2.0.5}$$

we get that $f'(y_2^*) = \tilde{\gamma} - r$, so y_2^* is stable if $\tilde{\gamma} < r$. However, determining the stability of the equilibrium for (2.0.1) is much more complicated because of the delay term.

Next, a Taylor expansion of equation (2.0.1) about the nonzero equilibrium point $y^* = y_2^*$ is performed. Considering the perturbation $u(t) = y(s) - y^*$ allows (2.0.1) to be rewritten in the following form:

$$\dot{u}(t) = f(u(t-1) + y^*, u(t-\tau) + y^*) \tag{2.0.6a}$$

$$\dot{u}(t) = \left(r - 2rc(\frac{r-\tilde{\gamma}}{cr})\right) u(t-1) - \tilde{\gamma}u(t-\tau) - rc(u(t-1))^2 \tag{2.0.6b}$$

which gives the following equation:

$$\dot{u}(t) = (2\tilde{\gamma} - r)u(t-1) - \tilde{\gamma}u(t-\tau) - rc(u(t-1))^2. \tag{2.0.7}$$

The Taylor expanion for the PMC model, found by Manjunath et al. [16], is

$$\dot{u}(t) = (2\gamma - rc_1)u(t-\tau) - \gamma u(t) - rc_2(u(t-\tau))^2. \tag{2.0.8}$$

It can be seen that the Taylor expanion of (2.0.1) is similar to that for the PMC model. The differences being caused by the appearance of the second delay with the $-\gamma$ term in (1.0.3), and by the replacements listed in (2.0.2).

The next step in analysing the stability of the nonzero equilibrium is looking at the characteristic equation. First linearizing (2.0.7) about the zero equilibrium gives

$$\dot{u}(t) = (2\tilde{\gamma} - r)u(t-1) - \tilde{\gamma}u(t-\tau). \tag{2.0.9}$$

Studying the nonzero equilibrium y_2^* of (2.0.1), is equivalent to studying the zero equilibrium of (2.0.7) obtained through a Taylor expansion about y_2^*.
Substituting in the ansatz $u(t) = e^{\lambda t}$ into (2.0.9) gives

$$\dot{u}(t) = \lambda e^{\lambda t} = (2\tilde{\gamma} - r)e^{\lambda(t-1)} - \tilde{\gamma}e^{\lambda(t-\tau)}, \tag{2.0.10}$$

and simplifying gives

$$\lambda = (2\tilde{\gamma} - r)e^{-\lambda} - \tilde{\gamma}e^{-\lambda\tau}. \tag{2.0.11}$$

As in [16], it will be considered that $\gamma > 0$, so $\tilde{\gamma} > 0$ and $rc_1 - 2\gamma = r - 2\tilde{\gamma} > 0$.

Now, using the characteristic equation above, it is possible to identify some region of stability, which will be done next, by the use of lemma 2.4 (which is similar to theorem 2.5 (ii)) in [15].

Theorem 2.1. (Li, Ruan and Wei [15]) *Suppose* $A \in (0,1)$ *and* $r_1 \leq \frac{1}{1+A}$. *Then all roots of*

$$\lambda = -e^{-\lambda r_1} - Ae^{-\lambda r_2} \tag{2.0.12}$$

have strictly negative real parts.

To apply theorem 2.1 above, equation (2.0.11) must first be rewritten in the form of (2.0.12). To do so, -1 is first factored out of the first coefficient, giving

$$\lambda = -(r - 2\tilde{\gamma})e^{-\lambda} - \tilde{\gamma}e^{-\lambda\tau}, \tag{2.0.13}$$

which after relabeling, setting $A_1 = r - 2\tilde{\gamma}$ and $A_2 = \tilde{\gamma}$, can be rewritten as

$$\lambda = -A_1e^{-\lambda} - A_2e^{-\lambda\tau}, \tag{2.0.14}$$

which satisfies the requirements from the paper that $A_1 > 0$ and $A_2 > 0$. Now, dividing both sides of (2.0.14) by A_1, and relabeling, gives the equation below to which theorem 2.1 can be applied

$$w = -e^{-wr_1} - Ae^{-wr_2}, \tag{2.0.15}$$

where $w = \frac{\lambda}{A_1}$, $A = \frac{A_2}{A_1}$, $r_1 = A_1$ and $r_2 = A_1\tau$. Now the conditions of theorem 2.1 are applied. From $A \in (0,1)$:

$$0 < \frac{\tilde{\gamma}}{r - 2\tilde{\gamma}} < 1 \tag{2.0.16}$$

which implies $3\tilde{\gamma} < r$, since it was already assumed $\tilde{\gamma} > 0$.

Now, using the second condition gives

$$r_1 = A_1 \leq \frac{1}{1 + \frac{A_2}{A_1}} = \frac{A_1}{A_1 + A_2}, \tag{2.0.17}$$

which simplifies as $1 \leq \frac{1}{r - \tilde{\gamma}}$, and after solving for r gives $r \leq 1 + \tilde{\gamma}$, since $r - \tilde{\gamma} > 0$ from the assumption $r - 2\tilde{\gamma} > 0$, which implies $r > 2\tilde{\gamma}$.

So after combining the two inequalities and applying theorem 2.1, it results that if

$$3\tilde{\gamma} < r \leq 1 + \tilde{\gamma} \tag{2.0.18}$$

then all roots of the characteristic equation (2.0.15) have strictly negative real parts. This implies that the positive equilibrium of (2.0.1) is asymptotically stable when r is in the above interval.

The system can undergo a Hopf bifurcation when (2.0.11) contains a pair of purely imaginary eigenvalues, $\lambda = \pm i\omega$, allowing the characteristic equation (2.0.11) to be written as

$$i\omega = (2\tilde{\gamma} - r)e^{-i\omega} - \tilde{\gamma}e^{-i\omega\tau}, \tag{2.0.19}$$

or, in the case where $\lambda = -i\omega$, as

$$-i\omega = (2\tilde{\gamma} - r)e^{i\omega} - \tilde{\gamma}e^{i\omega\tau}. \tag{2.0.20}$$

These two versions of the characteristic equation above will be used in later chapters, as well as the two expressions for parameters r and $\tilde{\gamma}$ in terms of ω and τ, which will now be found.

The process to obtain the previously mentioned expressions for parameters r and $\tilde{\gamma}$, uses the characteristic equation (2.0.19). After splitting the real and imaginary parts of (2.0.19), isolating the r in the real part, $0 = (2\tilde{\gamma} - r)\cos(\omega) - \tilde{\gamma}\cos(\omega\tau)$, gives

$$r = \frac{-\tilde{\gamma}\cos(\omega\tau) + 2\tilde{\gamma}\cos(\omega)}{\cos(\omega)}. \tag{2.0.21}$$

Substituting (2.0.21) into the imaginary part of (2.0.19) gives the equation

$$\omega + \frac{\tilde{\gamma}\cos(\omega\tau)\sin(\omega)}{\cos(\omega)} - \tilde{\gamma}\sin(\omega\tau) = 0, \tag{2.0.22}$$

from which $\tilde{\gamma}$ is isolated as

$$\tilde{\gamma} = \frac{-\omega\cos(\omega)}{\cos(\omega\tau)\sin(\omega) - \sin(\omega\tau)\cos(\omega)}. \tag{2.0.23}$$

Now that a region of stability for the positive equilibrium of (2.0.1), y_2^*, has been found, as well as equations for r and $\tilde{\gamma}$ at a Hopf bifurcation, this information can be combined in a plot. After setting, for example, $\tau = \frac{1}{3}$, Figures 2.1 and 2.2 were produced, showing only the positive axes, as $r, \tilde{\gamma} \geq 0$. Figure 2.1 shows the behaviour of the lines that form the bounds on the region where the nonzero equilibrium of (2.0.1) is stable (from (2.0.18)) in the $(r, \tilde{\gamma})$ plane, as well as three curves corresponding to $(r, \tilde{\gamma})(\omega)$, for three different intervals of ω. The red curve corresponds to $\omega \in [0.001, 9]$, the pink lines for when $\omega \in [9.8, 18]$, and the green curve to $\omega \in [19, 27]$.

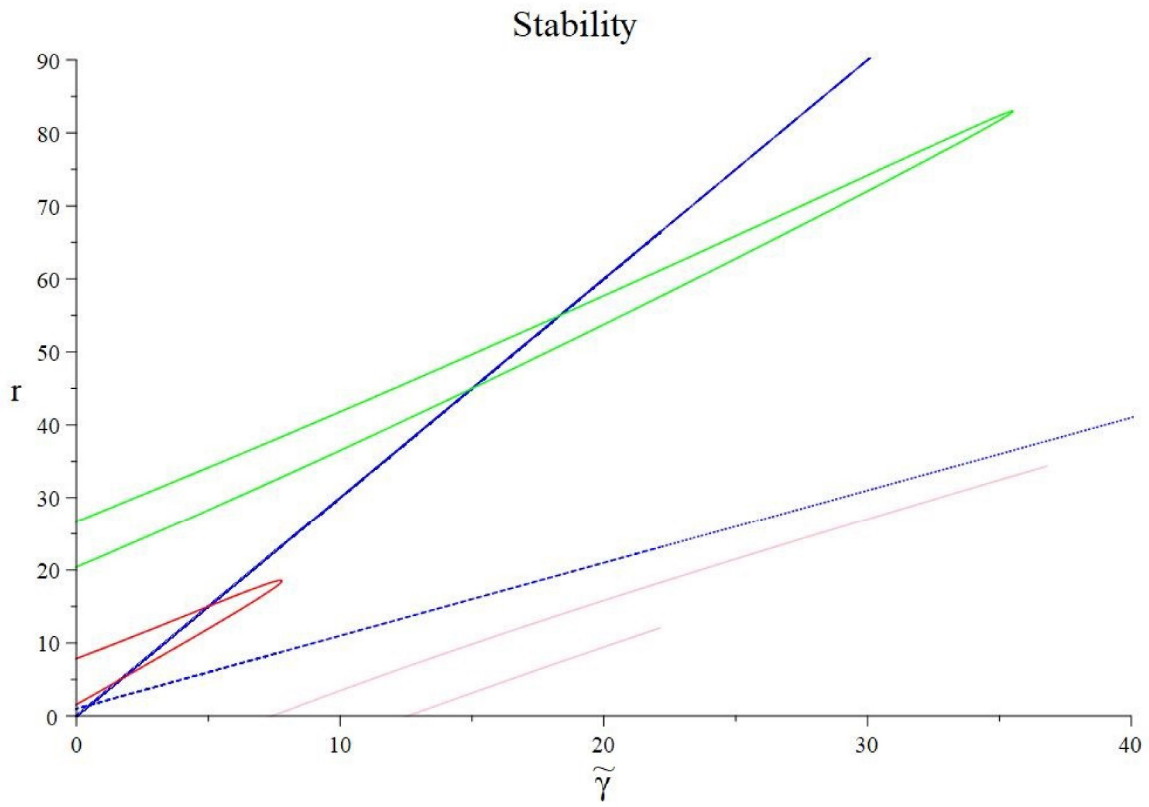

Figure 2.1: A plot of $3\tilde{\gamma}$ (solid blue line), $1+\tilde{\gamma}$ (shown as the dotted line) and r versus $\tilde{\gamma}$, for three intervals of ω. For the red curve, $\omega \in [0.001, 9]$, the pink corresponds to $\omega \in [9.8, 18]$, and for the green curve $\omega \in [19, 27]$.

The main region of interest however is near the lines that form the bounds on r, and the nearest Hopf bifurcation curve. The next plot shows a zoomed in version of Figure 2.1 into this region.

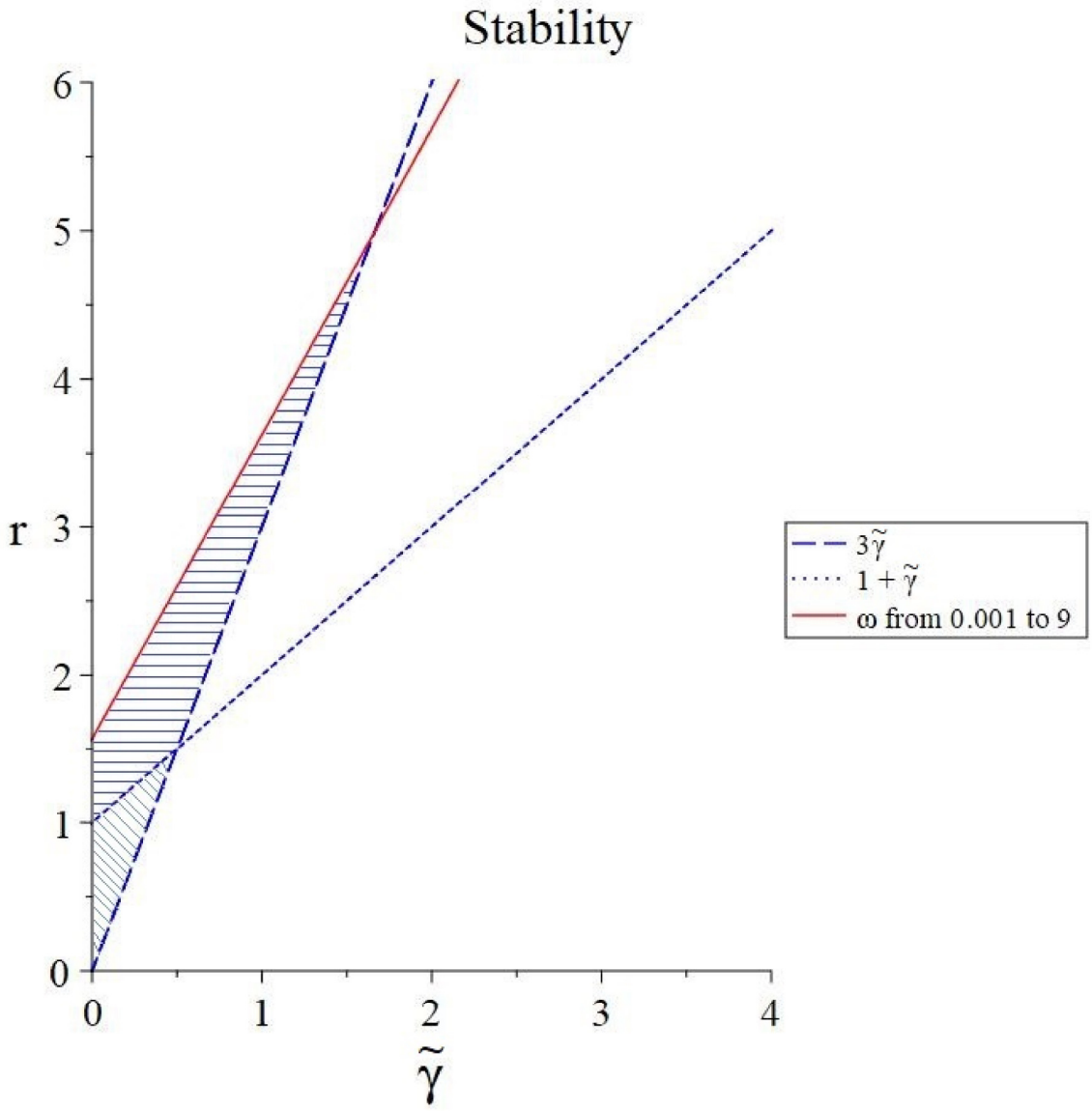

Figure 2.2: A plot of r for $\omega \in [0.001, 9]$, $3\tilde{\gamma}$ and $1 + \tilde{\gamma}$, by $\tilde{\gamma}$.

What can be seen in Figure 2.2 are the lines that form the bounds on r given in equation (2.0.18), as well as the lower branch of $(r, \tilde{\gamma})(\omega)$ for $\omega \in [0.001, 9]$, which also coincides with the interval from which ω is taken in a later chapter to gain more information about the behavior at the Hopf bifurcation. The lines are identified in the legend. In the plot, the upper, solid red line corresponds to $(r, \tilde{\gamma})$ at the Hopf bifurcation, so it represents the curve where the stability can change. The lower triangular region, identified by diagonal hash lines shows the region where the positive equilibrium of (2.0.1) is stable, according to the conditions in theorem 2.1 (Li, Ruan

and Wei). However, as the conditions of theorem 2.1, used to find this region, give sufficient but not necessary conditions for stability, it is not surprising that this plot shows the region of stability is actually larger, continuing up to the solid red line to include the region identified by the horizontal hash lines.

Chapter 3

Center Manifold and Normal Form

In Chapter 2, the focus was on finding a region of stability for the nonzero equilibrium of (2.0.1), given the existence of a Hopf bifurcation. Now, it remains to obtain more information about what happens at the Hopf bifurcation. In general, in the study of a DDE, first an ODE describing the flow on the center manifold is obtained, and then its normal form on the center manifold is found [6]. This chapter will focus on obtaining a pair of ordinary differential equations on the center manifold, through center manifold reduction applied to the DDE (2.0.7). To do so, the method described in [6] will be used. Next, the normal form of (2.0.7) in polar coordinates will be found using the formula from [7].

3.0.1 Center Manifold

In the study of DDEs, as for ODEs, it is often of interest (especially near a bifurcation point) to determine the behavior of the DDE or ODE near an equilibrium point, and in this pursuit the center manifold comes up. This section will focus on what a center manifold is, and why it would be useful, starting with the simpler case of an ODE as illustration.

In studying the dynamics near an equilibrium point, two important things to take into consideration are whether the system is linear or nonlinear, and whether the equilibrium is hyperbolic (no eigenvalues have zero real part [20]), or not. Throughout this subsection, the notation will mostly follow that in [20], sometimes from [24], while summarizing some information presented in [20, 24], unless another reference is given.

First, we will consider how one can study the behavior of solutions in the simpler case of linear ODEs. Considering a system of linear ODEs, written as $\dot{x} = Ax$, where $x \in \mathbb{R}^n$ and A is an $n \times n$ matrix, and has $x(0) = x_0$ as its initial condition, then this system will have $x(t) = e^{At}x_0$ as its unique solution $\forall t$. Finding the matrix e^{At} will usually require finding the eigenvalues of matrix A and their corresponding eigenvectors or generalized eigenvectors. At this point, the stable, unstable, and

center subspaces of $\dot{x} = Ax$ can be found. The solutions in these subspaces will behave in different ways, and knowing the make up of the subspaces of $\dot{x} = Ax$ allows one to determine the behavior of the solutions. In general, if $\lambda_j = a_j + ib_j$ are the eigenvalues of A, then the stable subspace, E^s, is the span of the s generalized eigenvectors of A which correspond to the s eigenvalues with $a_j < 0$. The span of the u generalized eigenvectors corresponding to the u eigenvalues having $a_j > 0$ form the unstable subspace E^u, and the center subspace, E^c, is then the span of the c generalized eigenvectors of A which correspond to eigenvalues having $a_j = 0$, and $s + u + c = n$. In all three cases, solutions that start in one subspaces will remain in that same subspace $\forall t$. On the stable subspace, solutions that start in E^s will tend to the origin $x = 0$ as $t \to \infty$, solutions starting in E^u will approach $x = 0$ as $t \to -\infty$, and the solutions in E^c, may or may not be bounded.

Now, we consider a nonlinear system, $\dot{x} = f(x)$, with $x \in \mathbb{R}^n$, and having x_0 as an equilibrium point. We define its linear part as $\dot{x} = Ax$, where $A = Df(x_0)$ is an $n \times n$, matrix of partial derivatives of f, evaluated at the equilibrium of interest, x_0. In the case of a hyperbolic equilibrium point (no eigenvalues have zero real part), determining the behavior near the equilibrium point is easier. Since generally the nonlinear system cannot be solved, the linear system near x_0 is studied to obtain information about the nonlinear system near the equilibrium point, a method supported by the Stable Manifold Theorem and the Hartman-Grobman theorem. They show that in the neighborhood of x_0 of $\dot{x} = f(x)$, solutions will behave as they would in a neighborhood of x_0 in the associated linear system. In summary, the Stable Manifold Theorem says that if A has k, and $n - k$ eigenvalues with negative and positive real parts, respectively, then there is a k-dimensional stable manifold S tangent to the stable subspace of the linear system, E^s, at x_0 and a $n - k$-dimensional unstable manifold U tangent to E^u of the linear system at x_0. The Hartman-Grobman Theorem says that there is a homeomorphism, H, which maps trajectories near x_0 of the nonlinear system onto trajectories of the corresponding linear system near x_0, so H can be used to find stable and unstable manifolds from E^s and E^u.

In the case of nonhyperbolic fixed points, determining the behavior of solutions becomes more complicated, since the behavior of solutions in the linearized system cannot be used to determine the behavior of solutions near x_0 for the original, nonlinear system. Considering a breakdown of eigenvalues as described for the subspaces of the linear system, then $\dot{x} = f(x)$ has a c-dimensional center manifold, tangent to E^c at x_0. The behavior of solutions on the center manifold near x_0, will determine their behavior in the original system, $\dot{x} = f(x)$, in a neighbourhood of x_0. Therefore, the nonlinear system can be restricted to the center manifold to study the dynamics near x_0, and the goal now becomes computing the center manifold. For a nonlinear system of the following form, following notation in [24],

$$\begin{aligned} \dot{x} &= Ax + f(x, y) \\ \dot{y} &= By + g(x, y), \end{aligned} \tag{3.0.1}$$

where $(x, y) \in \mathbb{R}^c \times \mathbb{R}^s$, A is a $c \times c$ matrix having eigenvalues that are purely imaginary, or zero, and B is a $s \times s$ matrix of eigenvalues having negative real parts, the method to do so involves a polynomial, $h(x)$. This polynomial, $h(x)$, is of degree equal to the level of accuracy needed for the center manifold, and must satisfy the equation

$$\mathcal{N}(h(x)) \equiv Dh(x)\left[Ax + f(x, h(x))\right] - Bh(x) - g(x, h(x)) = 0. \tag{3.0.2}$$

The flow on the center manifold is given by

$$\dot{x} = Ax + f(x, h(x)) \tag{3.0.3}$$

where $x \in \mathbb{R}^c$.

The above method for computing the center manifold applies to ODEs, but the procedure for finding the flow on the center manifold for DDEs is summarized in the following section.

3.0.2 Calculations

Now, the definitions and notations in [9] will be referred to, to place (2.0.7) in a proper functional setting. First, letting $\tau_m = \max\{1, \tau\}$, we define the Banach space, B, of continuous functions from $[-\tau_m, 0]$ into $\mathbb{R}^n$, as $B = C([-\tau_m, 0], \mathbb{R}^n)$. Then, by [9] the DDE in (2.0.7) can be written in the following form :

$$\dot{u}(t) = f(t, u_t), \tag{3.0.4}$$

where $u_t \in B$, with $u_t(\theta) = u(t + \theta)$ for $-\tau_m \leq \theta \leq 0$ for any $t \in [\sigma, \sigma + A]$, assuming $\sigma \in \mathbb{R}, A \geq 0$, and $u \in C([\sigma - \tau_m, \sigma + A], \mathbb{R}^n)$, with $f : D \to \mathbb{R}^n$ where D is a subset of $\mathbb{R} \times B$. The initial condition is taken as $u_0(\theta) \geq 0$.

Now, continuing with the method in [6], since the DDE to be considered is nonlinear, the linear and nonlinear terms can be separated as follows:

$$\dot{u}(t) = L(u_t) + F(u_t), \tag{3.0.5}$$

where $F \in C^N(B; \mathbb{R}^n)$, $N \geq 2$, $F(0) = 0$ and $DF(0) = 0$. Also $L : B \to \mathbb{R}^n$ is a bounded linear operator, meaning that there is an $n \times n$ matrix $\eta(\theta)$, with $-\tau_m \leq \theta \leq 0$ and having elements of bounded variation, so that

$$L(\phi) = \int_{-\tau_m}^{0} d[\eta(\theta)]\phi(\theta), \qquad \text{where } \phi \in B. \tag{3.0.6}$$

This implies that the linearization of (3.0.5) about the zero equilibrium,

$$\dot{u}(t) = L(u_t), \tag{3.0.7}$$

can be rewritten as

$$\dot{u}(t) = \int_{-\tau_m}^{0} d[\eta(\theta)]u(t+\theta). \tag{3.0.8}$$

For $\mathbb{R}^{n*}$, a space of row vectors of dimension n, letting $B^* = C([0,\tau_m];\mathbb{R}^{n*})$ allows the following bilinear form to be defined on $B^* \times B$:

$$\langle \psi, \phi \rangle = \psi(0)\phi(0) - \int_{-\tau_m}^{0}\int_{0}^{\theta} \psi(\xi-\theta)[d\eta(\theta)]\phi(\xi)d\xi \tag{3.0.9}$$

which, to be used for the purposes of (2.0.9), can be reduced as follows.
First, changing the order of integration, allows (3.0.9) to be rewritten as

$$\begin{aligned}\langle \psi, \phi \rangle &= \psi(0)\phi(0) - \int_{-\tau_m}^{0}\int_{\xi}^{-\tau_m} \psi(\xi-\theta)[d\eta(\theta)]\phi(\xi)d\xi \\ &= \psi(0)\phi(0) + \int_{-\tau_m}^{0}\int_{-\tau_m}^{\xi} \psi(\xi-\theta)[d\eta(\theta)]\phi(\xi)d\xi.\end{aligned} \tag{3.0.10}$$

The linearization of (2.0.7) at the equilibrium is given in equation (2.0.9), and to simplify notation, the following two substitutions will be made in equation (2.0.9): $a = 2\tilde{\gamma} - r$ and $b = -\tilde{\gamma}$. This gives

$$\dot{u}(t) = au(t-1) + bu(t-\tau), \tag{3.0.11}$$

allowing $d\eta(\theta)$ to be written as follows:

$$d\eta(\theta) = \big(a\delta(\theta+1) + b\delta(\theta+\tau)\big)\, d\theta, \tag{3.0.12}$$

where δ is the Dirac delta. So, then continuing from (3.0.10),

$$\begin{aligned}\langle \psi, \phi \rangle &= \psi(0)\phi(0) + \int_{-\tau_m}^{0}\int_{-\tau_m}^{\xi} \psi(\xi-\theta)\left(a\delta(\theta+1) + b\delta(\theta+\tau)\right) d\theta\phi(\xi)d\xi \\ &= \psi(0)\phi(0) + \int_{-1}^{0}\int_{-\tau_m}^{\xi} \psi(\xi-\theta)\left(a\delta(\theta+1)\right) d\theta\phi(\xi)d\xi \\ &+ \int_{-\tau}^{0}\int_{-\tau_m}^{\xi} \psi(\xi-\theta)\left(b\delta(\theta+\tau)\right) d\theta\phi(\xi)d\xi.\end{aligned} \tag{3.0.13}$$

Since $\delta(\theta+1) = 0$ unless $\theta = -1$ and $\delta(\theta+\tau) = 0$ unless $\theta = -\tau$, we get

$$\begin{aligned}\langle \psi, \phi \rangle = \psi(0)\phi(0) + a\int_{-1}^{0} \psi(\xi+1)\phi(\xi)d\xi \\ + b\int_{-\tau}^{0} \psi(\xi+\tau)\phi(\xi)d\xi.\end{aligned} \tag{3.0.14}$$

Before using (3.0.14), a few more definitions should be presented, which will be done in this paragraph, following the definitions in [6]. The generalized eigenspace, which will be labelled M_λ, corresponding to the eigenvalue λ must be considered, where λ satisfies the characteristic equation (2.0.11). Defining Λ, as in [6], as a nonempty finite set of eigenvalues, allows one to define P as $P = span\{M_\lambda : \lambda \in \Lambda\}$, of dimension m, where m represents the number of solutions to the characteristic equation which are in Λ. P also has a complementary space Q, so that there is a decomposition $B = P \oplus Q$. Then, we can define a basis for P as $\Phi = (\phi_1, \ldots, \phi_m)$, and Ψ is then defined as a basis for the dual space P^* in B^*, so that $\langle \Psi, \Phi \rangle = I_m$.

In summary, with this decomposition, $B = P \oplus Q$, we obtain the center manifold by projecting the solutions from the infinite dimensional space B onto the finite (m-dimensional) invariant space P, which is associated with the solutions to the characteristic equation (2.0.11) [6]. The center manifold, given by $h \in Q$ (h can be seen in equations (3.0.24), (3.0.25) and (3.0.27) farther down), is tangent to the space P at the equilibrium [6, 7]. So, as in the case of ODEs, the graph of h gives the center manifold, but the difference comes with how one finds h, either solving an algebraic equation in the case of ODEs, or solving differential equations for DDEs, which will become more evident in Chapter 6 [7, 24].

Continuing with the calculations, now equation (3.0.14) can be used to find Ψ. Given that at a Hopf bifurcation, we have

$$\Phi(\theta) = \begin{pmatrix} e^{i\omega_0\theta} & e^{-i\omega_0\theta} \end{pmatrix}, \tag{3.0.15}$$

and its dual basis is

$$\Phi(\theta)^T = \Psi' = \begin{pmatrix} e^{-i\omega_0\theta} \\ e^{i\omega_0\theta} \end{pmatrix}, \tag{3.0.16}$$

then

$$\psi(0)\phi(0) = \begin{pmatrix} 1 & 1 \\ 1 & 1 \end{pmatrix}. \tag{3.0.17}$$

The first integral in (3.0.14) gives

$$a\int_{-1}^{0} \psi(\xi+1)\phi(\xi)d\xi = a\begin{pmatrix} e^{-i\omega_0} & \frac{ie^{-i\omega_0} - ie^{i\omega_0}}{2\omega_0} \\ \frac{ie^{-i\omega_0} - ie^{i\omega_0}}{2\omega_0} & e^{i\omega_0} \end{pmatrix}. \tag{3.0.18}$$

The second integral in (3.0.14) gives

$$b\int_{-\tau}^{0}\psi(\xi+\tau)\phi(\xi)d\xi = b\begin{pmatrix} \tau e^{-i\omega_0\tau} & \frac{ie^{-i\omega_0\tau}-ie^{i\omega_0\tau}}{2\omega_0} \\ \frac{ie^{-i\omega_0\tau}-ie^{i\omega_0\tau}}{2\omega_0} & \tau e^{i\omega_0\tau}\end{pmatrix}. \tag{3.0.19}$$

Now, putting together equation (3.0.17), (3.0.18) and (3.0.19) into equation (3.0.14), with ψ' replacing ψ in (3.0.14), and simplifing the matrix entries by the use of the characteristic equations (2.0.19 - 2.0.20) gives

$$\begin{aligned}\langle\psi',\phi\rangle &= \begin{pmatrix} 1+ae^{-i\omega_0}+b\tau e^{-i\omega_0\tau} & 0 \\ 0 & 1+ae^{i\omega_0}+b\tau e^{i\omega_0\tau}\end{pmatrix} \\ &= \begin{pmatrix} 1+(2\tilde{\gamma}-r)e^{-i\omega_0}-\tilde{\gamma}\tau e^{-i\omega_0\tau} & 0 \\ 0 & 1+(2\tilde{\gamma}-r)e^{i\omega_0}-\tilde{\gamma}\tau e^{i\omega_0\tau}\end{pmatrix}.\end{aligned} \tag{3.0.20}$$

Taking the inverse of the above matrix gives

$$\langle\psi',\phi\rangle^{-1} = \begin{pmatrix} \frac{1}{1+(2\tilde{\gamma}-r)e^{-i\omega_0}-\tilde{\gamma}\tau e^{-i\omega_0\tau}} & 0 \\ 0 & \frac{1}{1+(2\tilde{\gamma}-r)e^{i\omega_0}-\tilde{\gamma}\tau e^{i\omega_0\tau}}\end{pmatrix}. \tag{3.0.21}$$

So now, we can determine Ψ, which can be found by the calculation of $\langle\psi',\phi\rangle^{-1}\Phi^T$ to give

$$\begin{aligned}\Psi(\theta) &= \begin{pmatrix} \frac{1}{1+(2\tilde{\gamma}-r)e^{-i\omega_0}-\tilde{\gamma}\tau e^{-i\omega_0\tau}} & 0 \\ 0 & \frac{1}{1+(2\tilde{\gamma}-r)e^{i\omega_0}-\tilde{\gamma}\tau e^{i\omega_0\tau}}\end{pmatrix}\begin{pmatrix} e^{-i\omega_0\theta} \\ e^{i\omega_0\theta}\end{pmatrix} \\ &= \begin{pmatrix} \frac{e^{-i\omega_0\theta}}{1+(2\tilde{\gamma}-r)e^{-i\omega_0}-\tilde{\gamma}\tau e^{-i\omega_0\tau}} \\ \frac{e^{i\omega_0\theta}}{1+(2\tilde{\gamma}-r)e^{i\omega_0}-\tilde{\gamma}\tau e^{i\omega_0\tau}}\end{pmatrix} = \begin{pmatrix}\psi_1(\theta) \\ \psi_2(\theta)\end{pmatrix},\end{aligned} \tag{3.0.22}$$

and at $\theta = 0$,

$$\Psi(0) = \begin{pmatrix} \frac{1}{1+(2\tilde{\gamma}-r)e^{-i\omega_0}-\tilde{\gamma}\tau e^{-i\omega_0\tau}} \\ \frac{1}{1+(2\tilde{\gamma}-r)e^{i\omega_0}-\tilde{\gamma}\tau e^{i\omega_0\tau}}\end{pmatrix}. \tag{3.0.23}$$

Now, we can find the flow on the center manifold, which is defined as

$$u_t = \Phi z(t) + h(z(t);F), \tag{3.0.24}$$

where $z(t)$ solves the following ODE:

$$\dot{z}(t) = Jz + \Psi(0)F(\Phi z + h(z;F)), \tag{3.0.25}$$

with J given by the 2×2 matrix

$$J = \begin{pmatrix} i\omega_0 & 0 \\ 0 & -i\omega_0 \end{pmatrix}. \tag{3.0.26}$$

The center manifold is given by

$$M_F = \{\phi \in B : \phi = \Phi z + h(z; F), \text{z in a neighbourhood of zero in } \mathbb{R}^m\}, \tag{3.0.27}$$

and for each z, $h(z; F) \in Q$ and is a C^n function of z, by the definition in [6].
So now, on the center manifold, letting $z = [z_1 \quad z_2]^T$, and using the nonlinear terms, $-rc(u(t-1))^2$ in equation (2.0.7), to write

$$F(v_1) = -rc(v_1(-1))^2, \tag{3.0.28}$$

so that on the center manifold, we get the following ordinary differential equations, using equation (3.0.25)

$$\begin{pmatrix} \dot{z}_1 \\ \dot{z}_2 \end{pmatrix} = \begin{pmatrix} i\omega_0 & 0 \\ 0 & -i\omega_0 \end{pmatrix} \begin{pmatrix} z_1 \\ z_2 \end{pmatrix} + \begin{pmatrix} \psi_1(0) \\ \psi_2(0) \end{pmatrix} F\left(\begin{pmatrix} e^{i\omega_0\theta} & e^{-i\omega_0\theta} \end{pmatrix} \begin{pmatrix} z_1 \\ z_2 \end{pmatrix} + h(z; F) \right), \tag{3.0.29}$$

so that

$$\begin{aligned} \dot{z}_1 &= i\omega_0 z_1 + \psi_1(0) \left[-rc(e^{-2i\omega_0} z_1^2 + 2z_1 z_2 + e^{2i\omega_0} z_2^2) + \mathcal{O}(|z|^3) \right] \\ \dot{z}_2 &= -i\omega_0 z_2 + \psi_2(0) \left[-rc(e^{-2i\omega_0} z_1^2 + 2z_1 z_2 + e^{2i\omega_0} z_2^2) + \mathcal{O}(|z|^3) \right]. \end{aligned} \tag{3.0.30}$$

Therefore, near the Hopf bifurcation, we now have the ODEs that $z(t)$ must solve in the equation giving the flow on the center manifold (3.0.24), which has a dimension of two. By restricting the flow to the center manifold, we now have a description of the behavior of the orbits of (2.0.7) near the zero equilibrium [6].

3.0.3 Normal Forms

Now that the flow has been restricted to the center manifold, the next step is to find normal forms in this center manifold [6].

In the simpler case of ODEs, after finding the system of differential equations that describe the flow on the center manifold (3.0.3), one can simplify the nonlinear part, using Normal Form Theory, to facilitate analysing the behavior of the nonlinear system, near the associated equilibrium point [20, 24]. We will refer to [20, 24] to give a brief summary on obtaining the normal form in the case of ODEs. To obtain the normal form of a system, we need the linear part of (3.0.3) in Jordan canonical form, represented by J, and a Taylor expansion of the nonlinear part, $F(x)$, resulting in a system of the form

$$\dot{x} = Jx + F_2(x) + F_3(x) + F_4(x) + \dots \tag{3.0.31}$$

where $x \in \mathbb{R}^n$. Then we simplify the nonlinear part, the $F_i(x)$, which is done step by step, increasing order, until a desired degree, by preforming a nonlinear change of coordinates at each step, of the form $x = y + h_i(y)$, where $h_i(y)$ is of order i, in y. At each step in this process, terms of order larger than i are modified, but the lower order terms will remain unchanged. To identify the terms that can be eliminated, the equation

$$L_J(h_i(y)) \equiv Jh_i(y) - Dh_i(y)Jy \tag{3.0.32}$$

is considered in the vector space H_i, the set of monomials of degree i. Choosing a space complementary to $L_J(H_i)$, labelled G_i, we can consider the decomposition $H_i = L_J(H_i) \oplus G_i$, and so the only terms of order i that remain in the normal form are in G_i. So the normal form is a simplified version of the original system, obtained through a coordinate transformation which allowed terms to be eliminated by the criteria described above.

In the case of DDEs, authors Faria and Magalhães have described methods for finding the normal forms for DDEs, with and without parameters, that do not require finding the center manifold at the equilibrium point first [6, 7].

Following line (3.12) of [7] allows the normal form of (3.0.30) on the center manifold for the Hopf bifurcation, to be written in polar coordinates as

$$\dot{\rho} = r\lambda'(0)\rho + K\rho^3 + \mathcal{O}(r^2\rho + |(\rho, r)|^4) \tag{3.0.33a}$$

$$\dot{\zeta} = -\omega + \mathcal{O}(|(\rho, r)|), \tag{3.0.33b}$$

where $\lambda'(0) = \frac{d(\mathrm{Re}\lambda(r))}{dr}|_{r=0}$ represents the speed and direction the eigenvalue, of the form $\lambda(r) = \alpha(r) + i\omega(r)$, is crossing the imaginary axis [7, 24]. This will be assumed to be positive since the eigenvalues are crossing from the stable region into the unstable region. Further, r is the bifurcation parameter, and K is the first Lyapunov coefficient which depends on all of the coefficients in (2.0.7), like τ and c, among others, and will be found in Chapter 5. The sign of K plays an important role in determining the behavior at a Hopf bifurcation, as we will see in the next two chapters.

Chapter 4

First Lyapunov Coefficient for PMC

This chapter will expand on the work done in [16] for the PMC model. While in [16], the authors give the expressions and formulas necessary for finding the Lyapunov coefficient, they do not explicitly write down the formula for the first Lyapunov coefficient, only saying that the expression is lengthy, and proceed to evaluate it numerically, for certain specific parameter values, finding that for the specified parameter values the Hopf bifurcation is supercritical and the resulting limit cycles are orbitally stable. In this chapter it will be proven that the first Lyapunov coefficient of the PMC model (equation (1.0.2)), is always negative or zero using the exact formula for K, which we will compute here.

Starting with (1.0.2), we can non-dimensionalize the model to decrease the number of parameters. This was done in Chapter 2 for equation (1.0.3), which is similar to the PMC model, the difference being the second delay. Therefore, the non-dimensionalized model corresponding to (1.0.2) will be the same as in (2.0.1), but without τ. More specifically it is

$$\dot{y}(s) = ry(s-1)(1-cy(s-1)) - \tilde{\gamma}y(s), \tag{4.0.1}$$

with the same substitutions that were made and resulted in equation (2.0.1), and so its Taylor expansion about the nonzero equilibrium is

$$\dot{u}(t) = (2\tilde{\gamma} - r)u(t-1) - \tilde{\gamma}u(t) - rc(u(t-1))^2. \tag{4.0.2}$$

4.0.1 Hopf Bifurcation

There are two types of Hopf bifurcation in (3.0.33a)-(3.0.33b) with $\tau = 0$, supercritical and subcritical. When $K < 0$, the Hopf bifurcation is supercritical (Figure 4.1) and the system goes from having a single, stable equilibrium, which looses stability after

the parameter increases past a critical value, and results in the appearance of a stable limit cycle [14]. In the case of a subcritical bifurcation (Figure 4.2), which corresponds to $K > 0$, the system goes from having an unstable limit cycle which disappears as the parameter increases past a critical value, and also the equilibrium stability changes from stable to unstable [14]. At the critical parameter value, the equilibrium is stable for a supercritical bifurcation but unstable in the case of a subcritical bifurcation [14]. Considering a parameter r, for which a Hopf bifurcation occurs at a critical value of r_0, two plots of the amplitude, by r, show the difference in behavior of a supercritical compared to a subcritical bifurcation.

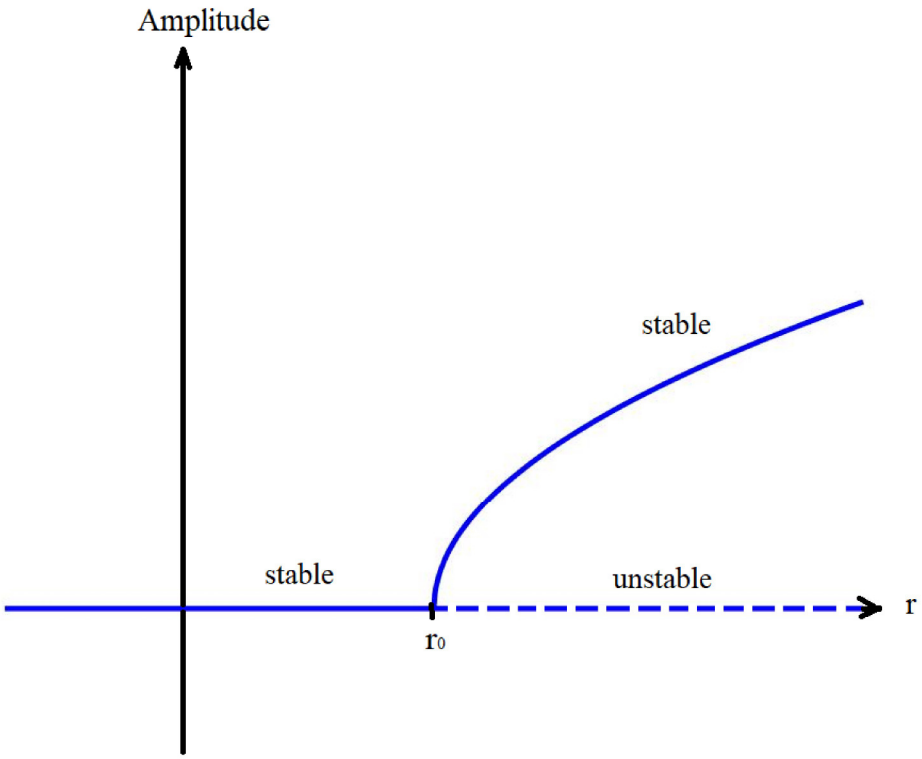

Figure 4.1: Supercritical Hopf bifurcation.

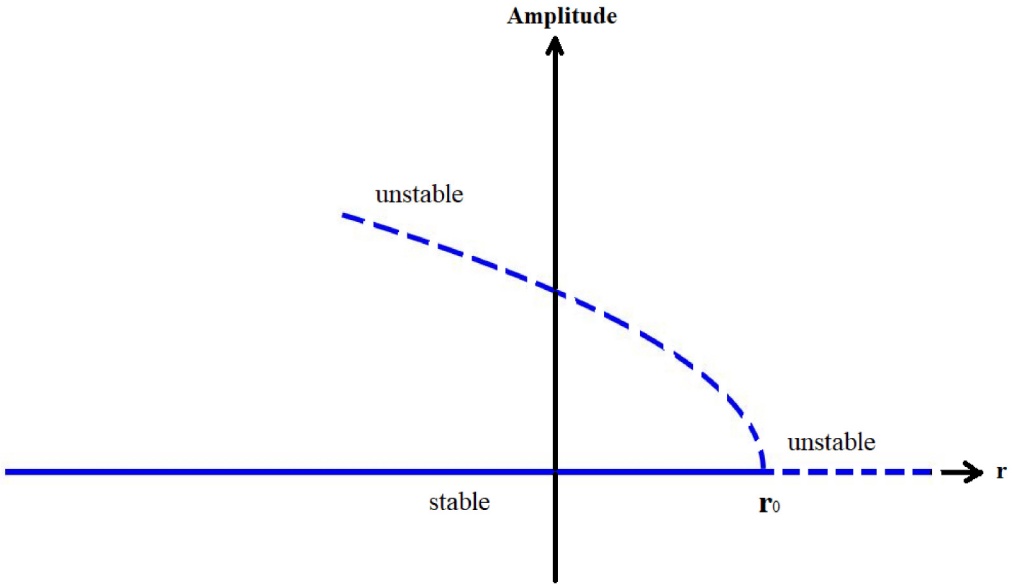

Figure 4.2: Subcritical Hopf bifurcation.

4.0.2 K for the PMC Model

In [7], it is shown (see equation (3.18) of that paper) that K in (3.0.33a) satisfies

$$K = Re\left[\frac{1}{1-L_0(\theta e^{i\omega\theta})}\left(B_{(2,1,0,0)} - \frac{B_{(1,1,0,0)}B_{(1,0,1,0)}}{L_0(1)} + \frac{B_{(2,0,0,0)}B_{(0,1,0,1)}}{2i\omega - L_0(e^{2i\omega\theta})}\right)\right] \tag{4.0.3}$$

when considering a DDE of the form of (3.0.5). L_0 is the linear part of $\dot{u}(t)$ in equation (4.0.2), and the nonlinear part is $F(u_t)$, and the $B_{(i,j,k,l)}$ are determined by the various coefficients in the DDE, which will be given in detail below. So, then

$$L_0(x) = (2\tilde{\gamma} - r)x(-1) - \tilde{\gamma}x(0) \tag{4.0.4}$$

and

$$F(x) = -rc(x(-1))^2. \tag{4.0.5}$$

Following formula (3.17) of [7]:

$$F(x_1e^{i\omega\theta} + x_2e^{-i\omega\theta} + x_31 + x_4e^{2i\omega\theta}, 0) = B_{(2,0,0,0)}x_1^2 + B_{(1,1,0,0)}x_1x_2 + B_{(1,0,1,0)}x_1x_3 + B_{(0,1,0,1)}x_2x_4 + B_{(2,1,0,0)}x_1^2x_2 + \dots, \tag{4.0.6}$$

we find the required $B_{(i,j,k,l)}$, after replacing θ with -1. So, the $B_{(i,j,k,l)}$ coefficients in (4.0.3) are found by reading off the coefficients which result from the following multiplication:

$$\begin{aligned} &- rc(x_1e^{-i\omega} + x_2e^{i\omega} + x_31 + x_4e^{-2i\omega})^2 \\ &= -rc(e^{-2i\omega}x_1^2 + 2x_1x_2 + 2e^{-i\omega}x_1x_3 + 2e^{-3i\omega}x_1x_4 + e^{2i\omega}x_2^2 \\ &+ 2e^{i\omega}x_2x_3 + 2e^{-i\omega}x_2x_4 + x_3^2 + 2e^{-2i\omega}x_3x_4 + e^{-4i\omega}x_4^2) \end{aligned} \tag{4.0.7}$$

so that:

$$B_{(2,1,0,0)} = 0 \qquad B_{(1,1,0,0)} = -2rc \tag{4.0.8}$$

$$B_{(1,0,1,0)} = -2rce^{-i\omega} \qquad B_{(2,0,0,0)} = -rce^{-2i\omega} \tag{4.0.9}$$

$$B_{(0,1,0,1)} = -2rce^{-i\omega}. \tag{4.0.10}$$

So now, to find K, the last terms needed in the equation are $L_0(1)$, $L_0(\theta e^{i\omega\theta})$, and $L_0(e^{2i\omega\theta})$, which are found using (4.0.4). First,

$$L_0(1) = \tilde{\gamma} - r. \tag{4.0.11}$$

For the following two terms, the characteristic equation of the PMC model, which from [16], is known to be (with the change in variables that produced the nondimensionalized model)

$$\lambda + \tilde{\gamma} + (r - 2\tilde{\gamma})e^{-\lambda} = 0, \tag{4.0.12}$$

will be used to simplify the terms, setting $\lambda = i\omega$ in (4.0.12). We get

$$\begin{aligned} L_0(\theta e^{i\omega\theta}) &= (2\tilde{\gamma} - r)(-e^{-i\omega}) - \tilde{\gamma}(0) \\ &= -(2\tilde{\gamma} - r)\frac{i\omega + \tilde{\gamma}}{(2\tilde{\gamma} - r)} \\ &= -\tilde{\gamma} - i\omega \end{aligned} \tag{4.0.13}$$

and

$$\begin{aligned} L_0(e^{2i\omega\theta}) &= (2\tilde{\gamma} - r)e^{-2i\omega} - \tilde{\gamma}(1) \\ &= (2\tilde{\gamma} - r)\left(\frac{i\omega + \tilde{\gamma}}{(2\tilde{\gamma} - r)}\right)^2 - \tilde{\gamma} \\ &= \frac{2i\omega\tilde{\gamma} - \tilde{\gamma}^2 - \omega^2 + \tilde{\gamma}r}{(2\tilde{\gamma} - r)} \quad \text{after simplifying.} \end{aligned} \tag{4.0.14}$$

Next, the program Maple is used to substitute equations (4.0.8) - (4.0.10), (4.0.11), and the last lines of (4.0.13) and (4.0.14) into the equation for K, (4.0.3). The number of parameters in K are reduced by using the characteristic equation (4.0.12) with $\lambda = i\omega$, to isolate r and $\tilde{\gamma}$, in a procedure similar to that explained in Chapter 2, which was used to obtain equations (2.0.21) and (2.0.23). Further simplifying gives the following formula for the first Lyapunov coefficient:

$$K = \frac{-16c^2\omega(\cos(\omega) - \frac{1}{2})^2 k_1(\omega)}{(4\cos(\omega) + 5)(\cos(\omega) - 1)(-\cos^2(\omega) - 2\cos(\omega)\sin(\omega)\omega + \omega^2 + 1)} \tag{4.0.15}$$

where

$$\begin{aligned} k_1(\omega) = &-2\cos^3(\omega)\sin(\omega) + (\omega + 2\sin(\omega))\cos^2(\omega) \\ &+ (-3\omega + \frac{13\sin(\omega)}{2})\cos(\omega) - \frac{11\omega}{2} + \sin(\omega). \end{aligned} \tag{4.0.16}$$

Theorem 4.1. *In the above expression for K (equation (4.0.15)), the first Lyapunov coefficient, K, is always smaller than or equal to zero.*

Proof: The first step will be to rewrite equation (4.0.15) slightly, to get rid of the fractions, and doing so, results in the following equation:

$$K = \frac{-2c^2\omega(2\cos(\omega) - 1)^2 P_1(\omega)}{(4\cos(\omega) + 5)(\cos(\omega) - 1)(2\cos(\omega)\sin(\omega)\omega - \omega^2 + \cos^2(\omega) - 1)} \tag{4.0.17}$$

where

$$\begin{aligned} P_1(\omega) = &\, 4\cos^3(\omega)\sin(\omega) - 2\omega\cos^2(\omega) - 4\sin(\omega)\cos^2(\omega) \\ &+ 6\omega\cos(\omega) - 13\sin(\omega)\cos(\omega) + 11\omega - 2\sin(\omega). \end{aligned} \tag{4.0.18}$$

The following steps involve determining the signs of each of the terms that are being multiplied together, starting with the denominator. It is known that $-1 \leq \cos(\omega) \leq 1$, $\forall\omega$, so for the first term being multiplied in the denominator:

$$\begin{aligned} -4+5 \leq 4\cos(\omega) \leq 4+5 \\ \text{which implies} \quad 1 \leq 4\cos(\omega)+5 \leq 9. \end{aligned} \tag{4.0.19}$$

Therefore, we know that $(4\cos(\omega)+5) \geq 0$, $\forall\omega$. Continuing in a similar way for the second term, we get

$$-2 \leq \cos(\omega) - 1 \leq 0, \tag{4.0.20}$$

meaning $(\cos(\omega)-1) \leq 0$, $\forall\omega$. Now, to determine the sign of the denominator, it remains to determine the sign of $(2\cos(\omega)\sin(\omega)\omega - \omega^2 + \cos^2(\omega) - 1)$, and to do so, it will be rewritten in the following way:

$$-\omega^2 + 2\cos(\omega)\sin(\omega)\omega + (\cos^2(\omega)-1) = \tag{4.0.21}$$
$$-\omega^2 + 2\cos(\omega)\sin(\omega)\omega + (-\sin^2(\omega)), \tag{4.0.22}$$

using the known identity $\sin^2(\omega)+\cos^2(\omega)=1$. Equation (4.0.22) can be considered as a quadratic-like function in ω, so its sign can be determined using the discriminant in the quadratic formula, b^2-4ac, given a quadratic ax^2+bx+c. So the discriminant of (4.0.22) is

$$\begin{aligned} 4\cos^2(\omega)\sin^2(\omega) - 4(-1)(-\sin^2(\omega)) &= 4\cos^2(\omega)\sin^2(\omega) - 4\sin^2(\omega) \\ &= 4\sin^2(\omega)(\cos^2(\omega)-1) \\ &= -4\sin^4(\omega) \leq 0. \end{aligned} \tag{4.0.23}$$

Since the discriminant is negative, we know (4.0.22) does not change sign, so that calculating the value of (4.0.22) at an $\omega > 0$ will be enough to determine its sign. Choosing $\omega = \frac{\pi}{2}$ gives $-(\frac{\pi}{2})^2 + 0 - 1 = -\frac{\pi^2+4}{4} < 0$. Therefore $(2\cos(\omega)\sin(\omega)\omega - \omega^2 + \cos^2(\omega) - 1) \leq 0$, meaning that the sign of the denominator is the product of $(+)(-)(-)$. Therefore the denominator of (4.0.17) is ≥ 0.

Now, it remains to look at the numerator of (4.0.17). Starting with $c^2 \geq 0$, and $(2\cos(\omega)-1)^2 \geq 0$ as squared terms are always positive in $\mathbb{R}$. We assume $\omega \geq 0$. So now, it remains to determine the sign of $P_1(\omega)$. There is a common factor of ω among some of the terms in $P_1(\omega)$, so equation (4.0.18) will be rewritten as

$$\begin{aligned} P_1(\omega) = \omega(6\cos(\omega) - 2\cos^2(\omega) + 11) \\ + 4\cos^3(\omega)\sin(\omega) - 4\cos^2(\omega)\sin(\omega) - 13\cos(\omega)\sin(\omega) - 2\sin(\omega). \end{aligned} \tag{4.0.24}$$

Dividing both sides of (4.0.24) by ω, and factoring out a $\sin(\omega)$, results in

$$\begin{aligned}\frac{P_1(\omega)}{\omega} &= (6\cos(\omega) - 2\cos^2(\omega) + 11) \\ &\quad + \frac{\sin(\omega)}{\omega}(4\cos^3(\omega) - 4\cos^2(\omega) - 13\cos(\omega) - 2).\end{aligned} \tag{4.0.25}$$

The next step is to split up the above equation into two parts A and B, identified as

$$A = -2\cos^2(\omega) + 6\cos(\omega) + 11 \tag{4.0.26}$$

and

$$B = 4\cos^3(\omega) - 4\cos^2(\omega) - 13\cos(\omega) - 2, \tag{4.0.27}$$

so that (4.0.25) can be rewritten as

$$\frac{P_1(\omega)}{\omega} = A + \frac{\sin(\omega)}{\omega}B. \tag{4.0.28}$$

Focusing first on A, since $-1 \leq \cos(\omega) \leq 1$, clearly we have $2\cos^2(\omega) - 6\cos(\omega) < 11$, so that $0 < A$.

Now, since determining when either the intercept of $P_1(\omega)$ (if we think of (4.0.24) as linear-like), or the term B, change signs is not helpful, the sign of terms $A + B$ and $A - B$ will be looked at. Starting with $A + B$, we find

$$A + B = 4\cos^3(\omega) - 6\cos^2(\omega) - 7\cos(\omega) + 9. \tag{4.0.29}$$

Letting $\cos(\omega) = x$, gives the following cubic polynomial, $f(x) = 4x^3 - 6x^2 - 7x + 9$, for which it can easily be seen that $x_1 = 1$ is a root. Through division by polynomials, dividing $f(x)$ by $(x - 1)$, gives

$$f(x) = (x - 1)(4x^2 - 2x - 9), \tag{4.0.30}$$

and applying the quadratic formula to the second factor gives the roots $x_2 = \frac{1}{4} - \frac{\sqrt{37}}{4}$, and $x_3 = \frac{1}{4} + \frac{\sqrt{37}}{4}$. Now, it will be determined on which intervals $f(x)$ is positive or negative, with the intervals given by the roots, as is shown in the table below.

	$x < \frac{1}{4} - \frac{\sqrt{37}}{4}$	$\frac{1}{4} - \frac{\sqrt{37}}{4} < x < 1$	$1 < x < \frac{1}{4} + \frac{\sqrt{37}}{4}$	$x > \frac{1}{4} + \frac{\sqrt{37}}{4}$
$(x - 1)$	-	-	+	+
$(4x^2 - 2x - 9)$	+	-	-	+
$A + B$	-	+	-	+

Table 4.1: Sign of $A + B$ by interval.

Since $x = \cos(\omega)$, $-1 \leq x \leq 1$, which fits inside the second interval $\frac{1}{4} - \frac{\sqrt{37}}{4} < x < 1$, from which it results that

$$A + B \geq 0 \quad \forall\omega \quad \text{or} \tag{4.0.31}$$
$$B \geq -A \quad \forall\omega. \tag{4.0.32}$$

Now, doing similarly for $A - B$, where

$$\begin{aligned} A - B &= -4\cos^3(\omega) + 2\cos^2(\omega) + 19\cos(\omega) + 13 \\ &= -4x^3 + 2x^2 + 19x + 13 = g(x) \quad (\text{if we let } \cos(\omega) = x\ ). \end{aligned} \tag{4.0.33}$$

After finding that $x_1 = -1$ is a root of $g(x)$, the division of this polynomial by $(x+1)$ allows $g(x)$ to be factored as

$$g(x) = (x+1)(-4x^2 + 6x + 13). \tag{4.0.34}$$

Using the quadratic formula, it can be found that the roots of $-4x^2 + 6x + 13$ are given by $x = \frac{-6 \pm \sqrt{244}}{-8}$, from which it results that $x_2 \approx -1.2026$ and $x_3 \approx 2.7026$. We determine the sign of $A - B$ on the intervals formed by its roots, using the table below.

	$x < -1.2026$	$-1.2026 < x < -1$	$-1 < x < 2.7026$	$x > 2.7026$
$(x+1)$	-	-	+	+
$(-4x^2 + 6x + 13)$	-	+	+	-
$A - B$	+	-	+	-

Table 4.2: Sign of $A - B$ by interval.

Since $x = \cos(\omega)$, the interval of interest is $-1 < x < 2.7026$, on which $A - B \geq 0$. Therefore, we get

$$A - B \geq 0 \quad \forall\omega \quad \text{or} \tag{4.0.35}$$
$$A \geq B \quad \forall\omega. \tag{4.0.36}$$

Combining (4.0.32) and (4.0.36) gives

$$-A \leq B \leq A \quad \forall\omega. \tag{4.0.37}$$

Going back to equation (4.0.28), we consider two cases, the first, when $B \geq 0$ and the second, when $B < 0$. Using that $-1 \leq \frac{\sin(\omega)}{\omega} \leq 1$ we get the following.

Case 1: When $B \geq 0$

$$\text{Starting with:} \quad -1 \leq \frac{\sin(\omega)}{\omega} \leq 1 \tag{4.0.38}$$

$$-1(B) \leq \frac{\sin(\omega)}{\omega} B \leq 1(B) \tag{4.0.39}$$

$$A - B \leq A + \frac{\sin(\omega)}{\omega} B \leq A + B \quad (\text{When } B \geq 0). \tag{4.0.40}$$

Therefore, since it was already determined that both $A + B \geq 0$ and $A - B \geq 0$, we know that $A + \frac{\sin(\omega)}{\omega} B \geq 0$ when $B \geq 0$.

Case 2: When $B < 0$

$$\text{Starting with:} \quad -1 \leq \frac{\sin(\omega)}{\omega} \leq 1 \tag{4.0.41}$$

$$-1(-B) \geq \frac{\sin(\omega)}{\omega}(-B) \geq 1(-B) \tag{4.0.42}$$

$$-A + B \geq -A - \frac{\sin(\omega)}{\omega} B \geq -A - B \tag{4.0.43}$$

$$-(A - B) \geq -(A + \frac{\sin(\omega)}{\omega} B) \geq -(A + B) \tag{4.0.44}$$

$$A - B \leq A + \frac{\sin(\omega)}{\omega} B \leq A + B \quad (\text{When } B < 0). \tag{4.0.45}$$

From where we get that $A + \frac{\sin(\omega)}{\omega} B \geq 0$, when $B < 0$, for the same reasons as mentioned in *Case 1.* Therefore, we get that $A + \frac{\sin(\omega)}{\omega} B = \frac{P_1(\omega)}{\omega} \geq 0$, $\forall \omega$, or, after multiplying both sides of the equation by ω, that

$$P_1(\omega) = \omega(A + \frac{\sin(\omega)}{\omega} B) \geq 0 \quad \forall \omega \text{ (since it was assumed that } \omega \geq 0). \tag{4.0.46}$$

So now we can find the sign of the numerator of equation (4.0.17) to be the product of $(-2)(+)(+)(+)(+)$, concluding that the numerator is ≤ 0. Therefore, we get

$$K = \frac{-}{+} \leq 0 \quad \forall \omega. \tag{4.0.47}$$

∎

Setting $c = 1$ to have K be a function of ω only, and using Maple to plot K by ω, shown in Figure 4.3, confirms that the first Lyapunov coefficient is always smaller than or equal to zero.

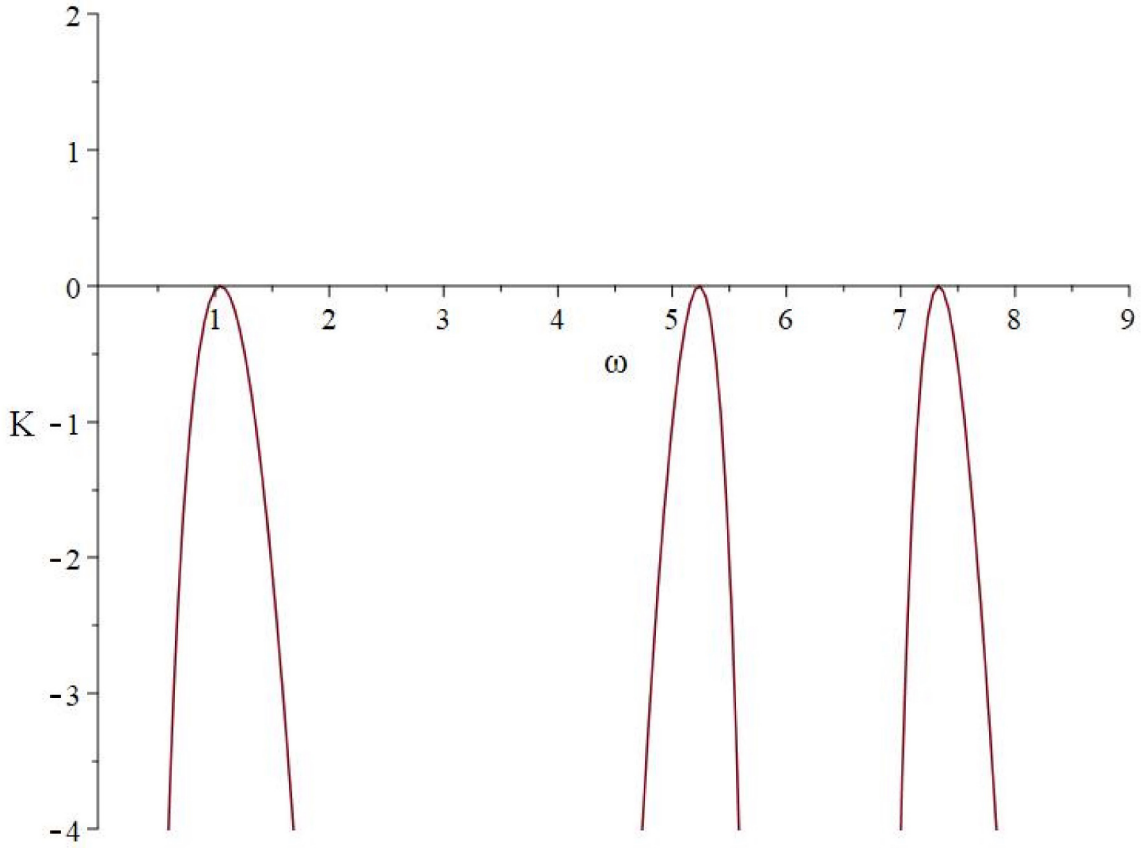

Figure 4.3: A plot of the first Lyapunov coefficient K, by ω.

At this point, theorem (3.20) in [7] can be used to draw the following conclusion about the PMC model. Assuming that the characteristic equation (4.0.12) obtained from the Taylor expansion of (4.0.1) about the nonzero equilibrium has $\pm i\omega$ as its only complex roots having the real part equal zero, and $K \neq 0$, then since $\lambda'(0)K < 0$ (since $\lambda'(0)$ is assumed positive) by this theorem in [7], we know there is a unique nontrivial periodic orbit when $r > 0$, having stable nontrivial periodic solutions. So, in other words, the Hopf bifurcation is always supercritical for the PMC model (except for the points where $K = 0$). This conclusion is the same as that obtained in [16] for specific parameter values, but the work in this chapter shows that that conclusion holds $\forall\omega$ (excluding the points where $K = 0$).

Chapter 5

First Lyapunov Coefficient for Model Under Study

Continuing on where Chapter 3 left off, this chapter will focus on finding the first Lyapunov coefficient of the main equation under study in this thesis, equation (2.0.1). So K from equation (3.0.33a), with $\tau \neq 0$, will now be found. As in Chapter 4, the first Lyapunov coefficient will be found by using the formula for K shown as equation (4.0.3). Recalling the Taylor expansion about the nonzero equilibrium of (2.0.1) shown as equation (2.0.7), we can now define

$$L_0(x) = (2\tilde{\gamma} - r)x(-1) - \tilde{\gamma}x(-\tau) \tag{5.0.1}$$

from the linear part of (2.0.7), and the nonlinear part gives

$$F(x) = -cr(x(-1))^2. \tag{5.0.2}$$

In this case, the $B_{(i,j,k,l)}$ coefficients are found by replacing θ with -1 in formula 3.17 of [7], and reading off the coefficients which result from the following multiplication, as in Chapter 4:

$$\begin{aligned} &- rc(x_1e^{-i\omega} + x_2e^{i\omega} + x_3 1 + x_4e^{-2i\omega})^2 \\ &= -rc(e^{-2i\omega}x_1^2 + 2x_1x_2 + 2e^{-i\omega}x_1x_3 + 2e^{-3i\omega}x_1x_4 + e^{2i\omega}x_2^2 \\ &+ 2e^{i\omega}x_2x_3 + 2e^{-i\omega}x_2x_4 + x_3^2 + 2e^{-2i\omega}x_3x_4 + e^{-4i\omega}x_4^2) \end{aligned} \tag{5.0.3}$$

to give

$$B_{(2,1,0,0)} = 0 \qquad B_{(1,1,0,0)} = -2rc \tag{5.0.4}$$

$$B_{(1,0,1,0)} = -2rce^{-i\omega} \qquad B_{(2,0,0,0)} = -rce^{-2i\omega} \tag{5.0.5}$$

$$B_{(0,1,0,1)} = -2rce^{-i\omega}. \tag{5.0.6}$$

Now, equation (5.0.1) will be used to find $L_0(1)$, $L_0(\theta e^{i\omega\theta})$, and $L_0(e^{2i\omega\theta})$.

$$L_0(1) = (2\tilde{\gamma} - r)(1) - \tilde{\gamma}(1) = \tilde{\gamma} - r, \tag{5.0.7}$$

$$\begin{aligned} L_0(\theta e^{i\omega\theta}) &= (2\tilde{\gamma} - r)(-e^{-i\omega}) - \tilde{\gamma}(-\tau e^{-i\omega\tau}) \\ &= -(2\tilde{\gamma} - r)e^{-i\omega} + \tilde{\gamma}\tau\frac{(-i\omega + (2\tilde{\gamma} - r)e^{-i\omega})}{\tilde{\gamma}} \\ &= (2\tilde{\gamma} - r)e^{-i\omega}(\tau - 1) - i\omega\tau \end{aligned} \tag{5.0.8}$$

and

$$\begin{aligned} L_0(e^{2i\omega\theta}) &= (2\tilde{\gamma} - r)(e^{-2i\omega}) - \tilde{\gamma}(e^{-2i\omega\tau}) \\ &= (2\tilde{\gamma} - r)e^{-2i\omega} - \tilde{\gamma}\frac{(-i\omega + (2\tilde{\gamma} - r)e^{-i\omega})^2}{\tilde{\gamma}^2} \\ &= \frac{-2\tilde{\gamma}^2 e^{-2i\omega} + 3\tilde{\gamma}re^{-2i\omega} + \omega^2 + 2i\omega e^{-i\omega}(2\tilde{\gamma} - r) - r^2e^{-2i\omega}}{\tilde{\gamma}}. \end{aligned} \tag{5.0.9}$$

To obtain the last two formulas the characteristic equation in (2.0.19) was used, isolating $e^{-i\omega\tau}$. Next, equations (5.0.4) - (5.0.9) are substituted into the formula for K using Maple. Then the characteristic equation is used to reduce the number of parameters, by deriving the expressions for r and $\tilde{\gamma}$ as explained in Chapter 2 and appear as equations (2.0.21) and (2.0.23), which are then substituted into K. The resulting formula for K is too lengthy to reproduce here. However, for illustrative purposes, letting $c = 1$ and $\tau = \frac{1}{3}$, gives the following expression for K in terms of ω:

$$K = \frac{M_1(\omega)}{M_2(\omega)} \tag{5.0.10}$$

where

$$\begin{aligned} M_1(\omega) = -3\omega\Big(8\cos^2\left(\frac{\omega}{3}\right) - 7\Big)^2\Big[&256\cos^{10}\left(\frac{\omega}{3}\right)\omega + 768\cos^9\left(\frac{\omega}{3}\right)\sin\left(\frac{\omega}{3}\right) \\ &+ 192\cos^9\left(\frac{\omega}{3}\right)\omega + 576\cos^8\left(\frac{\omega}{3}\right)\sin\left(\frac{\omega}{3}\right) - 768\cos^8\left(\frac{\omega}{3}\right)\omega \\ &- 1920\cos^7\left(\frac{\omega}{3}\right)\sin\left(\frac{\omega}{3}\right) - 544\cos^7\left(\frac{\omega}{3}\right)\omega - 1344\cos^6\left(\frac{\omega}{3}\right)\sin\left(\frac{\omega}{3}\right) \\ &+ 752\cos^6\left(\frac{\omega}{3}\right)\omega + 1488\cos^5\left(\frac{\omega}{3}\right)\sin\left(\frac{\omega}{3}\right) + 476\cos^5\left(\frac{\omega}{3}\right)\omega \\ &+ 900\cos^4\left(\frac{\omega}{3}\right)\sin\left(\frac{\omega}{3}\right) - 260\cos^4\left(\frac{\omega}{3}\right)\omega - 444\cos^3\left(\frac{\omega}{3}\right)\sin\left(\frac{\omega}{3}\right) \end{aligned}$$

$$- 114\cos^3\left(\frac{\omega}{3}\right)\omega - 174\cos^2\left(\frac{\omega}{3}\right)\sin\left(\frac{\omega}{3}\right) + 37\cos^2\left(\frac{\omega}{3}\right)\omega$$
$$+ 57\sin\left(\frac{\omega}{3}\right)\cos\left(\frac{\omega}{3}\right) + 3\cos\left(\frac{\omega}{3}\right)\omega + 3\sin\left(\frac{\omega}{3}\right)\Big]$$

and

$$M_2(\omega) = -8\sin^2\left(\frac{\omega}{3}\right)\left[8\cos^4\left(\frac{\omega}{3}\right) + 6\cos^3\left(\frac{\omega}{3}\right) - 4\cos^2\left(\frac{\omega}{3}\right) - 2\cos\left(\frac{\omega}{3}\right) + 1\right]$$
$$\times \left[8\cos^4\left(\frac{\omega}{3}\right)\omega^2 + 24\cos^3\left(\frac{\omega}{3}\right)\sin\left(\frac{\omega}{3}\right)\omega - 9\cos^2\left(\frac{\omega}{3}\right)\omega^2\right.$$
$$\left. - 18\cos\left(\frac{\omega}{3}\right)\sin\left(\frac{\omega}{3}\right)\omega + 9\cos^2\left(\frac{\omega}{3}\right) - 9\right].$$

Clearly the expression for K for equation (2.0.7), which has two delays, is lengthier than that for the PMC model. While for the PMC model, it was possible to show that the first Lyapunov coefficient is always zero or negative, a plot of the first Lyapunov coefficient of (2.0.7), apppearing as Figure 5.1, shows that in this case ($\tau = \frac{1}{3}$ and $c = 1$) it changes sign.

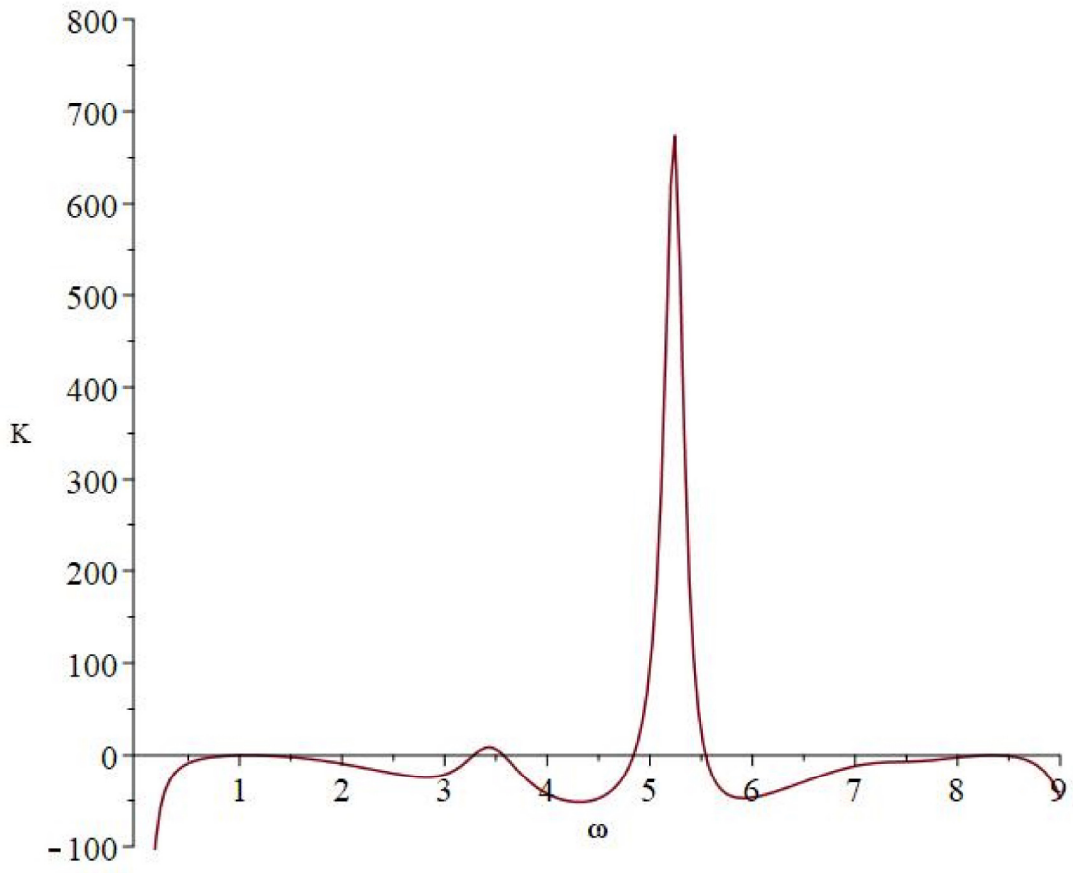

Figure 5.1: A plot of the first Lyapunov coefficient K, versus ω.

The changing sign of K means that the Hopf bifurcation can be either supercritical or subcritical, depending on the value of ω. Since K passes through zero, changing sign, for those values, higher order terms in the normal form are needed to gain more information about the behaviour of solutions near the zero equilibrium point of (2.0.7) [7]. For this reason the Bautin bifurcation will be considered in the next chapter.

Chapter 6

Second Lyapunov Coefficient

A Hopf bifurcation with the first Lyapunov coefficient equal to zero is degenerate and called a Bautin bifurcation. In order to properly analyze this bifurcation one needs to compute the so-called second Lyapunov coefficient [14]. Since it was determined in the previous chapter that the first Lyapunov coefficient of our model changes sign, the focus in this chapter will be to obtain information about the second Lyapunov coefficient, and determining if there are values of ω where the first and second Lyapunov coefficient have different signs, since this leads to multi-stability.

In general, in polar coordinates, the normal form for a Hopf bifurcation is a system of the following form,

$$\dot{\rho} = r\lambda^{'}(0)\rho + K_2\rho^3 + ... + K_{2p}\rho^{2p+1} + \mathcal{O}(r\rho\,|(\rho, r)| + |(\rho, r)|^{2p+2}) \tag{6.0.1a}$$

$$\dot{\zeta} = -\omega + \mathcal{O}(|(\rho, r)|), \tag{6.0.1b}$$

which needs to be computed up to the first K_{2p} coefficient such that $K_{2p} \neq 0$ [7].

Refering back to Chapter 5, when the first Lyapunov coefficient crosses the x-axis, $K = 0$ (corresponding to $K_2 = 0$ in (6.0.1a)), the second Lyapunov coefficient must be found. Therefore, the normal form, in polar coordinates, of the system that will be the focus of this chapter is:

$$\dot{\rho} = r\lambda^{'}(0)\rho + K\rho^3 + K_4\rho^5 + \mathcal{O}(r\rho\,|(\rho, r)| + |(\rho, r)|^6) \tag{6.0.2a}$$

$$\dot{\zeta} = -\omega + \mathcal{O}(|(\rho, r)|), \tag{6.0.2b}$$

where K is as stated in equation (5.0.10) of Chapter 5. For the cases when $K \approx 0$, we now want to find the second Lyapunov coefficient K_4.

6.0.1 Bautin Bifurcation

An equilibrium undergoes a Bautin bifurcation when it has $\lambda = \pm i\omega$ as eigenvalues and the first Lyapunov coefficient is zero, resulting in a Hopf bifurcation that turns, from supercritical to subcritical, or subcritical to supercritical [14]. For a Hopf bifurcation to turn from supercritical to subcritical, the first Lyapunov coefficient is negative while the second is positive, a behavior which is shown in Figure 6.1 as a plot of amplitude by r. When the first Lyapunov coefficient is positive and the second Lyapunov coefficient is negative is when the Hopf bifurcation turns from subcritical to supercritical, as shown in Figure 6.2. When both the first and second Lyapunov coefficients are negative, or positive, we expect a behavior similar to that shown in Figure 4.1 and 4.2 of Chapter 4, respectively, and so we do not expect the appearance of a second limit cycle in these cases because there is no change in the type of Hopf bifurcation.

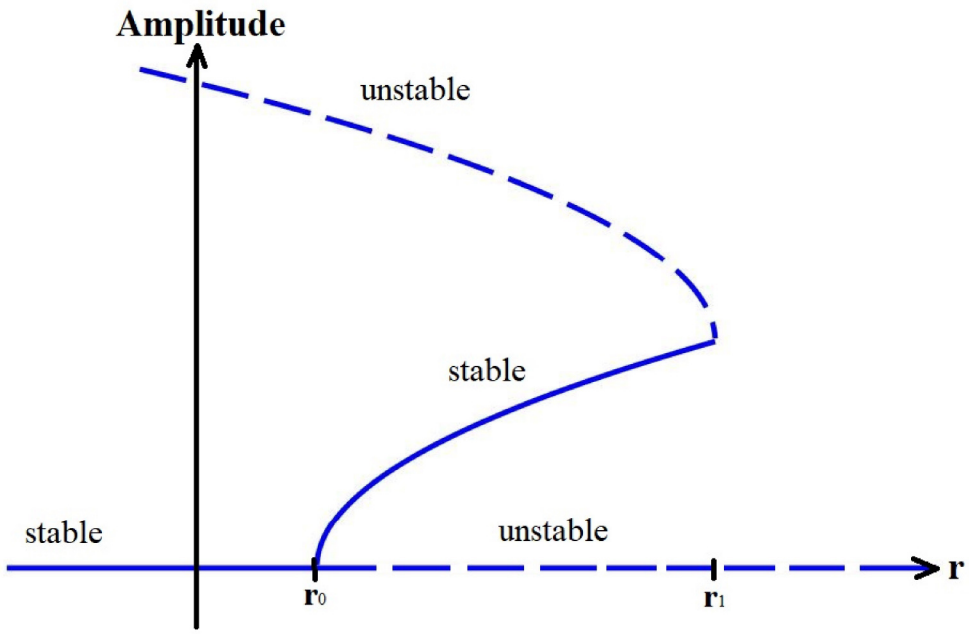

Figure 6.1: Behavior at the Bautin bifurcation, where the Hopf bifurcation turns from supercritical to subcritical.

What can be seen from Figure 6.1, is that when $r < r_0$, we have a stable equilibrium and an unstable limit cycle, so that solutions within the limit cycle will converge to the equilibrium, while those starting outside the limit cycle will not converge. For r between r_0 and r_1, we have an unstable equilibrium, and two limit cycles, a stable limit cycle inside an unstable limit cycle. When r is within this interval, solutions starting within the unstable limit cycle will converge to the stable limit cycle, while

solutions starting outside of this outer limit cycle will not converge. For $r > r_1$, we are left with an unstable equilibrium, which means that the solutions will not converge.

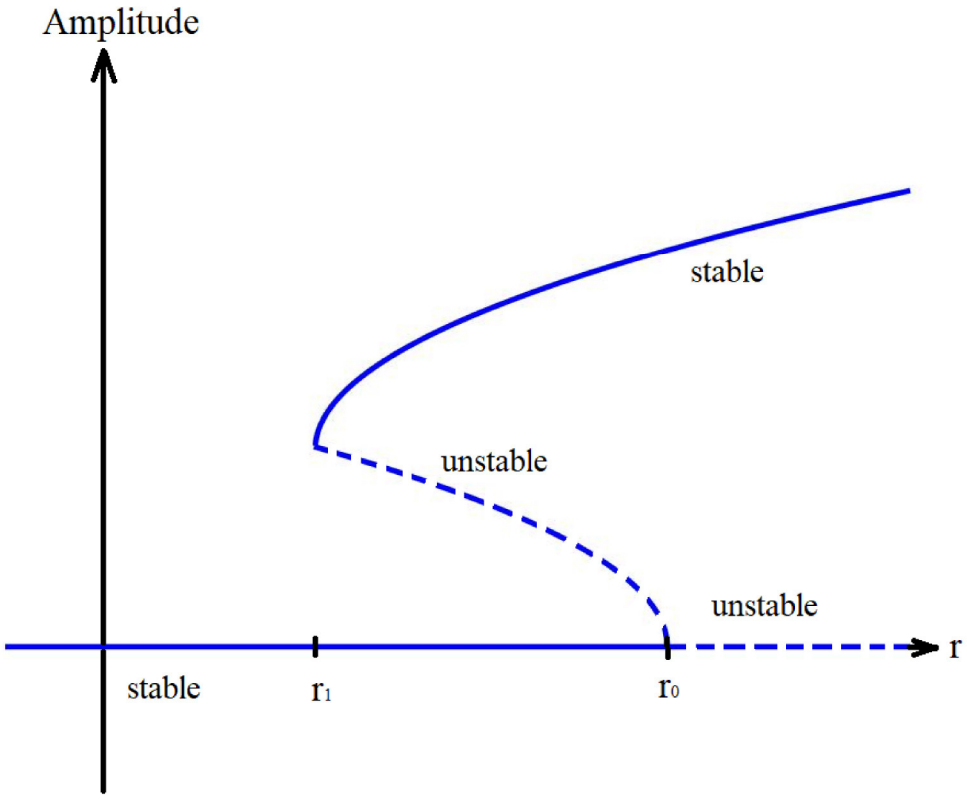

Figure 6.2: Behavior at the Bautin bifurcation, where the Hopf bifurcation turns from subcritical to supercritical.

From Figure 6.2, it can be seen that when $r < r_1$, we have a stable equilibrium. For r between r_1 and r_0, we see multi-stability. We have a stable equilibrium, and two limit cycles, an unstable limit cycle inside a stable limit cycle. When r is within this interval, solutions starting inside the unstable limit cycle will tend to the equilibrium, while solutions starting outside of the inner, unstable limit cycle will converge to the stable, outer, limit cycle, so that the behavior observed in the solutions depends on the initial condition. For $r > r_0$, the inner limit cycle disappears, via a subcritical Hopf bifurcation, while the equilibrium looses stability, so now, all solutions converge to the limit cycle. At this type of bifurcation, we see that solutions can jump from one stable equilibrium to another, which is characteristic of a phenomenon called *hysteresis* [14].

Therefore, we can see that in order to get a better understanding of the behavior of solutions near the nonzero equilibrium of (2.0.1), we need to find this second

Lyapunov coefficient because the behavior of solutions near the equilibrium has the potential to be more complicated than what is suggested by the first Lyapunov coefficient alone.

6.0.2 Finding the Second Lyapunov Coefficient

To find K_4, the procedure and definitions from [7] and [6] will be used, unless otherwise indicated. To do so, we will need to calculate higher order terms in normal form relative to an invariant space, P, which is the same as that defined in Chapter 3 [7]. This section continues from where Chapter 3, Section *Calculations*, ended. So, we want to find the higher order terms in equations (3.0.30) from Chapter 3.

The normal form relative to this invariant space P, that we are looking for is of the form

$$\dot{x} = Jx + \frac{1}{2!}g_2^1(x) + \frac{1}{3!}g_3^1(x) + \frac{1}{4!}g_4^1(x) + \frac{1}{5!}g_5^1(x) + \mathcal{O}(|x|^6), \tag{6.0.3}$$

where we need to find the coefficients $g_j^1(x)$. In studying the Hopf bifurcation, not all the coefficients in order j are needed. In this case, when $j = 3$, we only need to find the coefficient in front of the term $z^2\bar{z}$. Also, in normal form, we know that the second-order and fourth-order terms can be eliminated [24]. For the fifth degree terms, it can be found that only the coefficient in front of $z^3\bar{z}^2$ is needed.

Refering back to equation (3.0.5), and the related definitions in Chapter 3, we now consider the infinitesimal generator A_0, associated to the solutions of $\dot{u}(t) = L(u_t)$, and satisfies the relation $A_0\varphi = \dot{\varphi}$ [6].

P is the invariant space for A_0, associated with $\Lambda \neq \emptyset$, a finite set, consiting of the eigenvalues of A_0, and since it is of interest to find the normal forms on the center manifold, we want that the $\lambda \in \Lambda$ satisfy $Re(\lambda) = 0$. For normal forms, an appropriate phase space needs to be considered, which in this case means considering equation (3.0.5) as an abstract ODE in the Banach space JB, made up of functions from $[-\tau_m, 0] \to \mathbb{R}^n$, which are uniformly continuous on $[-\tau_m, 0)$, having a jump discontinuity at 0. This abstract ODE is of the following form:

$$\frac{d}{dt}v = Av + X_0F(v) \tag{6.0.4}$$

when separating linear and nonlinear parts, where $A\varphi = \dot{\varphi} + X_0[L(\varphi) - \dot{\varphi}(0)]$ having domain B^1, a subset of JB,

$$X_0 = \begin{cases} I & \text{if } \theta = 0 \\ 0 & -\tau_m \leq \theta < 0 \end{cases}$$

and in this case

$$L(\varphi) = (2\tilde{\gamma} - r)\varphi(-1) - \tilde{\gamma}\varphi(-\tau). \tag{6.0.5}$$

Then define $\pi : JB \to P$, where $JB = P \oplus Ker(\pi)$ with $Q \subsetneqq Ker(\pi)$, as

$$\pi(\varphi + X_0\alpha) = \Phi[(\Psi, \varphi) + \Psi(0)\alpha]. \tag{6.0.6}$$

Restricting A from B^1 to $Q^1 = Ker(\pi) \cap B^1$, and labelling this as A_{Q^1}, then equation (6.0.4) can be represented by the following system:

$$\begin{aligned} \dot{x} &= Jx + \Psi(0)F(\Phi x + y) \\ \dot{y} &= A_{Q^1}y + (I - \pi)X_0F(\Phi x + y), \end{aligned} \tag{6.0.7}$$

where $x \in \mathbb{R}^m$ and $y \in Q^1$. Here, $x = \begin{pmatrix} z \\ \bar{z} \end{pmatrix}$, and we recall from Chapter 3 that

$$J = \begin{pmatrix} i\omega_0 & 0 \\ 0 & -i\omega_0 \end{pmatrix} \tag{6.0.8}$$

and we found that

$$\Psi(0) = \begin{pmatrix} \frac{1}{1+(2\tilde{\gamma}-r)e^{-i\omega_0} - \tilde{\gamma}\tau e^{-i\omega_0\tau}} \\ \frac{1}{1+(2\tilde{\gamma}-r)e^{i\omega_0} - \tilde{\gamma}\tau e^{i\omega_0\tau}} \end{pmatrix} = \begin{pmatrix} \psi_1 \\ \psi_2 \end{pmatrix}. \tag{6.0.9}$$

The terms needed in equation (6.0.3) are obtained using a recursive procedure, where for each term we use the lower order terms in the normal form which have already been found, and those of the same order from the original equation, using the formulas in equation (6.0.7). To find these higher order terms we first consider a change of variables of the form

$$\begin{aligned} x &= \bar{x} + p(\bar{x}) \\ y &= \bar{y} + h(\bar{x}). \end{aligned} \tag{6.0.10}$$

After computing the normal form, up to order j, and ignoring the bars, equations (6.0.7) can be written as:

$$\begin{aligned} \dot{x} &= Jx + \sum_{i=2}^{j} \frac{1}{i!} g_i^1(x, y) + \dots \\ \dot{y} &= A_{Q^1}y + \sum_{i=2}^{j} \frac{1}{i!} g_i^2(x, y) + \dots \end{aligned} \tag{6.0.11}$$

where to find $g_i^1(x, y)$ we use that $g_i^1(x, y) = \Psi(0)F_i(\Phi x + y) - D_x p(x)Jx + Jp(x)$ where the F_i are the terms from the Taylor expansion of the nonlinear terms in (6.0.4). In the equation for $\dot{y}$, we set $g_i^2(x, y) = 0$, which results in the following equation

$$D_x h(x)Jx - A_{Q^1}h(x) = (I-\pi)X_0F(\Phi x + y), \tag{6.0.12}$$

which becomes:

$$D_x h(x)Jx - \dot{h} + X_0[Lh - \dot{h}(0)] = X_0F(\Phi x + y) - \Phi\Psi(0)F(\Phi x + y) \tag{6.0.13}$$

where, for each j,

$$h = \sum_{|(q,l)|=j-1} h_{q,l}z^q\bar{z}^l \quad \text{where } h_{q,l} \in Q^1 \tag{6.0.14}$$

and

$$F_j(\Phi x) = \sum_{|(q,l)|=j} A_{(q,l)}z^q\bar{z}^l. \tag{6.0.15}$$

For example, the ones that are needed here are, in the case of $j = 3$, we use $h(\theta) = h_{2,0}(\theta)z^2 + h_{1,1}(\theta)z\bar{z} + h_{0,2}(\theta)\bar{z}^2$, and when $j = 4$ we use $h(\theta) = h_{3,0}(\theta)z^3 + h_{2,1}(\theta)z^2\bar{z} + h_{1,2}(\theta)z\bar{z}^2 + h_{0,3}(\theta)\bar{z}^3$, and when $j = 5$, we use $h(\theta) = h_{4,0}(\theta)z^4 + h_{3,1}(\theta)z^3\bar{z} + h_{2,2}(\theta)z^2\bar{z}^2 + h_{1,3}(\theta)z\bar{z}^3 + h_{0,4}(\theta)\bar{z}^4$. Here, the $A_{(q,l)}$ in (6.0.15) are the coefficients of the $z^q\bar{z}^l$ that result from the multiplication in equation (6.0.16).

Recalling the nonlinear term in the Taylor expansion, $-rc(u(t-1))^2$, here we consider:

$$\begin{aligned} F(\Phi x + h) = -rc\Big(&e^{-i\omega}z + e^{i\omega}\bar{z} + h_{2,0}(-1)z^2 + h_{1,1}(-1)z\bar{z} \\ &+ \cdots + h_{2,2}(-1)z^2\bar{z}^2 + h_{1,3}(-1)z\bar{z}^3 + h_{0,4}(-1)\bar{z}^4\Big)^2. \end{aligned} \tag{6.0.16}$$

Therefore, at each step we work on the equation for $\dot{x}$, which affects the differential equations we then solve from $\dot{y}$, which in turn affects the higher order terms on $\dot{x}$, and the process repeats until we reach the order we desire in normal form. Using equation (6.0.13), we find the differential equations that need to be solved, and their initial conditions. The differential equations are given by

$$D_x hBx - \frac{dh}{d\theta} = -\Phi\Psi(0)F(\Phi x + y), \tag{6.0.17}$$

while the initial conditions are given by

$$L(h) - \dot{h}(0) = F(\Phi x + y). \tag{6.0.18}$$

For example, the second-order differential equations that need to be solved are:

$$\begin{aligned} \dot{h}_{2,0}(\theta) - 2i\omega h_{2,0}(\theta) &= -rc(\psi_1 e^{i\omega_0\theta} e^{-2i\omega_0} + \psi_2 e^{-i\omega_0\theta} e^{-2i\omega_0}) \\ \dot{h}_{1,1}(\theta) &= -rc(2\psi_1 e^{i\omega_0\theta} + 2\psi_2 e^{-i\omega_0\theta}) \\ \dot{h}_{0,2}(\theta) + 2i\omega_0 h_{0,2}(\theta) &= -rc(\psi_1 e^{i\omega_0\theta} e^{2i\omega_0} + \psi_2 e^{-i\omega_0\theta} e^{2i\omega_0}), \end{aligned} \tag{6.0.19}$$

which have the following initial conditions

$$\begin{aligned} (2\tilde{\gamma} - r)h_{2,0}(-1) - \tilde{\gamma}h_{2,0}(-\tau) - \dot{h}_{2,0}(0) &= -rc(e^{-2i\omega_0}) \\ (2\tilde{\gamma} - r)h_{1,1}(-1) - \tilde{\gamma}h_{1,1}(-\tau) - \dot{h}_{1,1}(0) &= -2rc \\ (2\tilde{\gamma} - r)h_{0,2}(-1) - \tilde{\gamma}h_{0,2}(-\tau) - \dot{h}_{0,2}(0) &= -rc(e^{2i\omega_0}). \end{aligned} \tag{6.0.20}$$

Putting all this into code in Maple, which was written by my supervisor, we get a very lengthy formula for the second Lyapunov coefficient.

After, a few more lines of code were written, in Maple, that divides the interval of $\omega \in [1, 5]$ into 100 points, and at each of those 100 points, the value of the first and second Lyapunov coefficients, K and K_4, respectively, were calculated and then plotted, resulting in Figure 6.3. It should be noted that the values for K are as indicated by the y-axis, but the values for K_4 have been scaled, so that the values for K_4 are actually 1000 times larger than indicated by the y-axis. This was done so the that shape of K is visible when plotted alongside K_4.

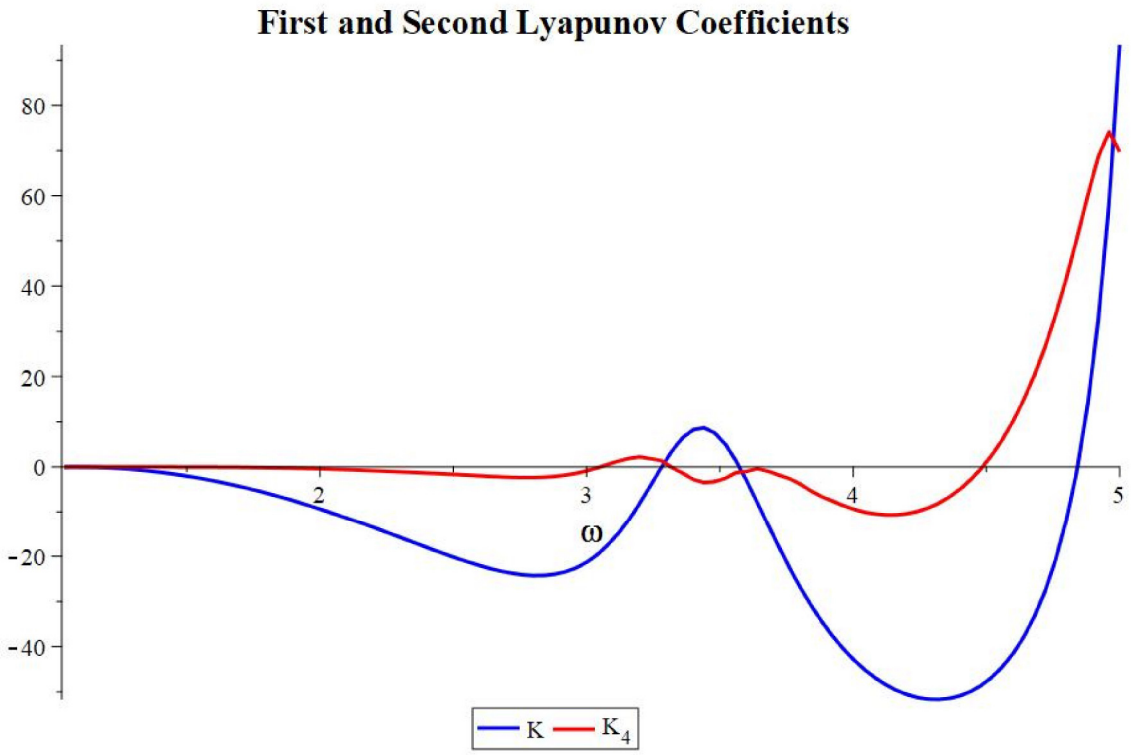

Figure 6.3: A plot of the first Lyapunov coefficient K, and second Lyapunov coefficient K_4, versus ω. The scale for K_4 is such that 1 unit = 1000.

As can be seen from Figure 6.3, one of the points where the first Lyapunov coefficient crosses the x-axis (the blue curve) is a bit after $\omega = 3.5$, at which point the second Lyapunov coefficient (red curve) is negative. At $\omega = 3.5$, so before $K = 0$, the first Lyapunov coefficient is positive, so that the Hopf bifurcation is subcritical, and when $K = 0$, the second Lyapunov coefficient is negative, implying that at a certain value, r_1, the Hopf bifurcation will turn from subcritical to supercritical, so that the behavior expected in a plot of amplitude by r, is as shown in Figure 6.2.

So, because of the differing signs of the Lyapunov coefficients around $\omega = 3.5$ this value of ω is considered an interesting point at which to study the behavior of (2.0.1), which will be done using numerical simulations in the next chapter.

Chapter 7

Numerical Simulations

This chapter will focus on numerical simulations that help confirm some of the results obtained in Chapters 4, 5 and 6, for both the PMC model (4.0.1), and the main model under study, shown as equation (2.0.1). Throughout this chapter, the method used to compute the value of the solutions, $x(t)$, at time t, is the Forward Euler method used with $\Delta t = 0.001$, for a chosen initial condition defined for t in the interval $[-1, 0]$. The method is implemented using the program R, and the code can be found in Appendix B.

7.0.1 PMC model

In Chapter 4 it was shown that for the PMC model, the Hopf bifurcation is supercritical $\forall\omega$. As an example, choosing $\omega = 2.1$, and using Maple and the characteristic equation, it was found that in this case, at the Hopf bifurcation, $\tilde{\gamma} = 1.228180394$ and $r = 4.889142546$. Still assuming that $c = 1$ in equation (4.0.1), we obtain Figure 7.1, which shows a plot of amplitude by corresponding r value, where r is taken from 4.7 and increased to 5.2, by 0.01 at each step, and the amplitude is calculated at each r value. To obtain this plot, the starting initial condition was taken as $x(t) = 0.75$ for $t \in [-1, 0]$, after which it was taken as $x(t)$ for $t \in [99, 100]$ from the previous plot of $x(t)$ by t. As would be expected at a supercritical bifurcation, like that illustrated in Chapter 4 (Figure 4.1), the solutions have an amplitude of zero until a critical parameter value, r_0, after which the amplitude grows, and solutions start converging to the stable limit cycle. From this plot it appears that this critical value, r_0, where the Hopf bifurcation occurs is between 4.88 and 4.89, and it can be seen that this interval contains the theoretical value computed by Maple as the value of r at the Hopf bifurcation.

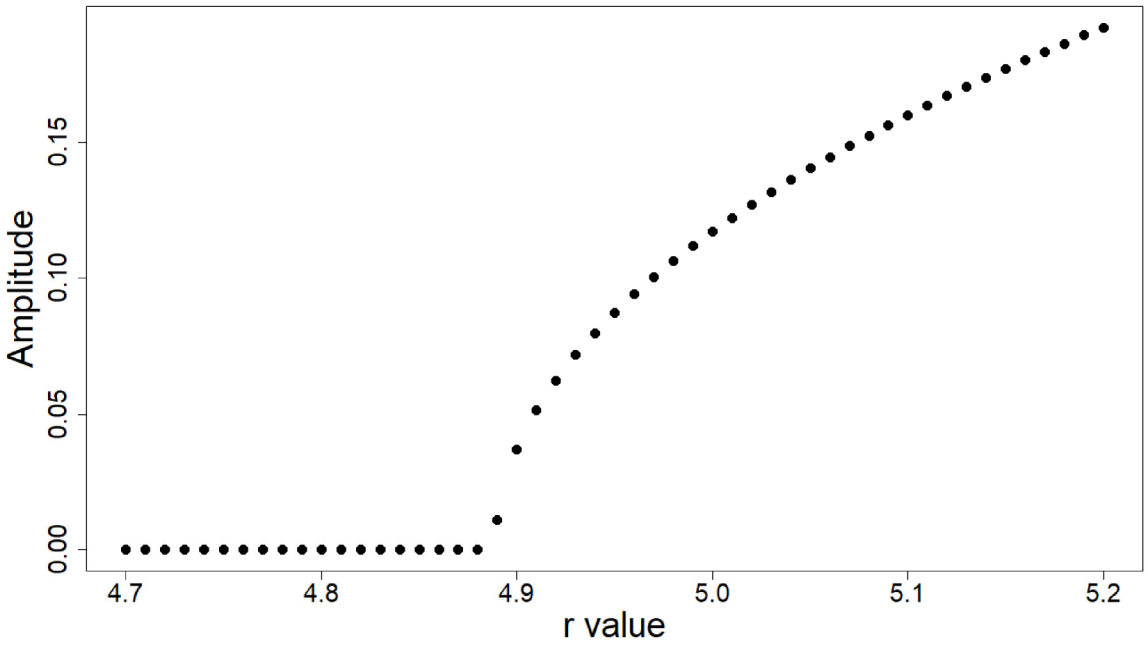

Figure 7.1: A plot of amplitude by r value, when $\omega = 2.1$ for (4.0.1).

Now it would be of interest to look at plots of the solutions, $x(t)$, by time, for values of r before and after the Hopf bifurcation, while keeping all other parameters the same. In both cases the x-axis, which is taken from -1 to T, is split up into intervals of 0.001 (since $\Delta t = 0.001$ in the Forward Euler method), to evaluate x at each indexed time, and T is chosen depending on how long is needed for the solution behavior to stabilize. Still considering the case of $\omega = 2.1$, we first take $r = 4.7 < r_0$. Here the time interval for t was taken as $[-1, 200]$, as this was considered long enough to determine the behaviour of the solutions. As can be seen from Figure 7.2, though the solutions are oscillating at the begining, they appear to converge to the equilibrium fairly quickly, resulting in an amplitude of zero.

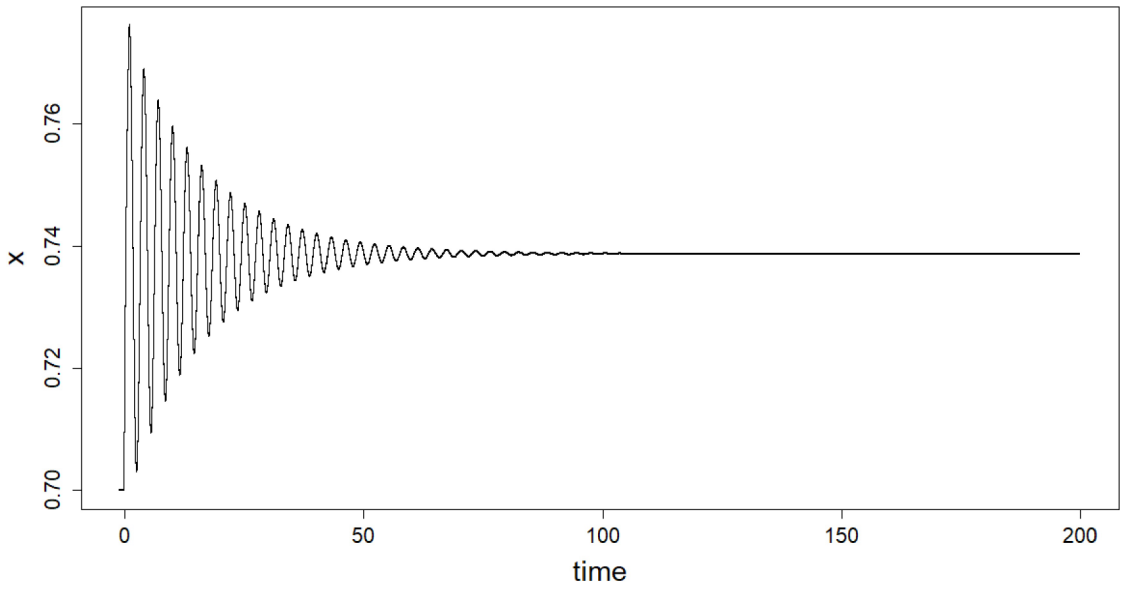

Figure 7.2: A plot of $x(t)$ by time, when $r = 4.7$.

In the second plot, Figure 7.3, when $r = 5 > r_0$, and $T = 300$, the solutions are clearly oscillating about the equilibrium, then grow in amplitide, and appear to converge to a nonzero amplitude fairly quickly. The behavior of the solutions shown in both plots are as expected from a supercritical Hopf bifurcation, and considering Figure 7.1.

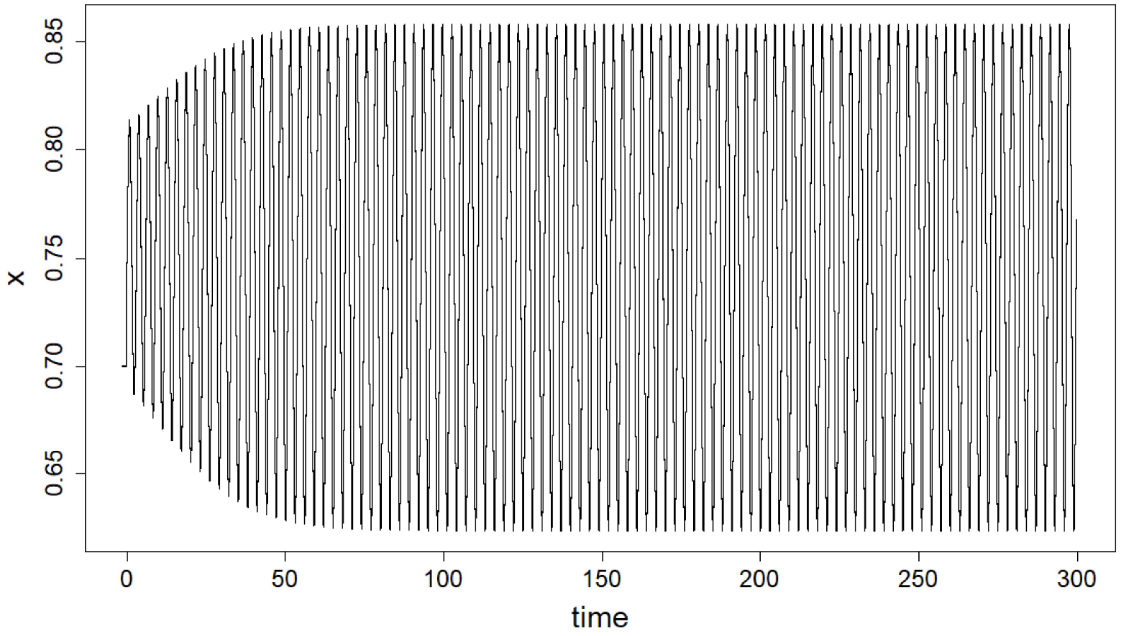

Figure 7.3: A plot of $x(t)$ by time, when $r = 5$.

In both cases the initial condition was set as the constant $x(t) = 0.7$ for $t \in [-1, 0]$, chosen to be not too far from the equilibrium values. When $r = 4.7$, the equilibrium is $\frac{4.7-1.228180394}{4.7} \approx 0.7387$, and when $r = 5$, the equilibrium will be $\frac{5-1.228180394}{5} \approx 0.7544$.

Therefore, the plots above suggest that the nonzero equilibrium of the PMC model is stable, until a value of r between 4.88 and 4.89, or perhaps $r = 4.889142546$ as calculated by Maple, when the system undergoes a Hopf bifurcation, after which this equilibrium looses stability and solutions start converging to a stable limit cycle. This confirms the results of Chapter 4 which classified the Hopf bifurcation for the PMC model as supercritical.

7.0.2 Main Model

Now, focusing on the main model under study, in equation (2.0.1), with $\tau = \frac{1}{3}$, the interest is in determining the behavior of the Hopf bifurcation when first and second Lyapunov coefficients have different signs. Looking at Figure 6.3 in Chapter 6, we can see that $\omega = 3.5$ would be good to investigate, since at this point, the first Lyapunov coefficient is positive and fairly close to where it crosses the x-axis, while the second Lyapunov coefficient is negative. Using the characteristic equation and Maple, we find that at this point, $\tilde{\gamma} = 4.532792698$ and $r = 10.96890755$.

The first two numerical simulation shown in Figures 7.4 to 7.5 are plots of amplitude by corresponding r value where the amplitude values were obtained in two different ways. In both cases, the amplitude, defined by $\frac{max(x)-min(x)}{2}$, is found for the corresponding values of r, ranging from 10.967 to 10.9836, by increments of 0.0001. For each value of r, $x(t)$ is calculated for $t \in [-1, 100]$ followed by the amplitude, and then its values for $x(t)$ in the interval $[99, 100]$ is used as the initial condition for the next $x(t)$, for $t \in [-1, 100]$ plot, followed by a calculation of the amplitude. While the difference between the last two amplitude values is greater than 0.00001, this process continues, until the difference between the last two amplitudes is ≤ 0.00001, and the last amplitude that was calculated becomes the amplitude for that r value.

The two methods differ through their initial conditions. For the first method, which produced Figure 7.4, we started near the limit cycle, and then while decreasing r, the amplitude is calculated, through the method described above. To be able to start on the limit cycle, for $r = 10.990$, $x(t)$ is calculated for $t \in [-1, 100]$, with original initial condition of $x(t) = 0.6$ when $t \in [-1, 0]$, and again, its values for $x(t)$ of the previous plot on the interval $[99, 100]$ is used as the initial condition on $[-1, 0]$ for the next plot of $x(t)$, for $t \in [-1, 100]$, and this is done 100 times. From this last plot, its values for $x(t)$ on the interval $[99, 100]$ are taken as the initial condition for the first r (10.9836). In Figure 7.4 we see that when we start near the limit cycle, and slowly decrease r, the solutions start by converging to the limit cycle, and the amplitude drops off to zero by $r = 10.9684$, which is slightly to the left of the theoretical value for the Hopf bifurcation computed by Maple. This suggests that when $r \leq 10.9684$, the nonzero equilibrium of equation (2.0.1) becomes stable.

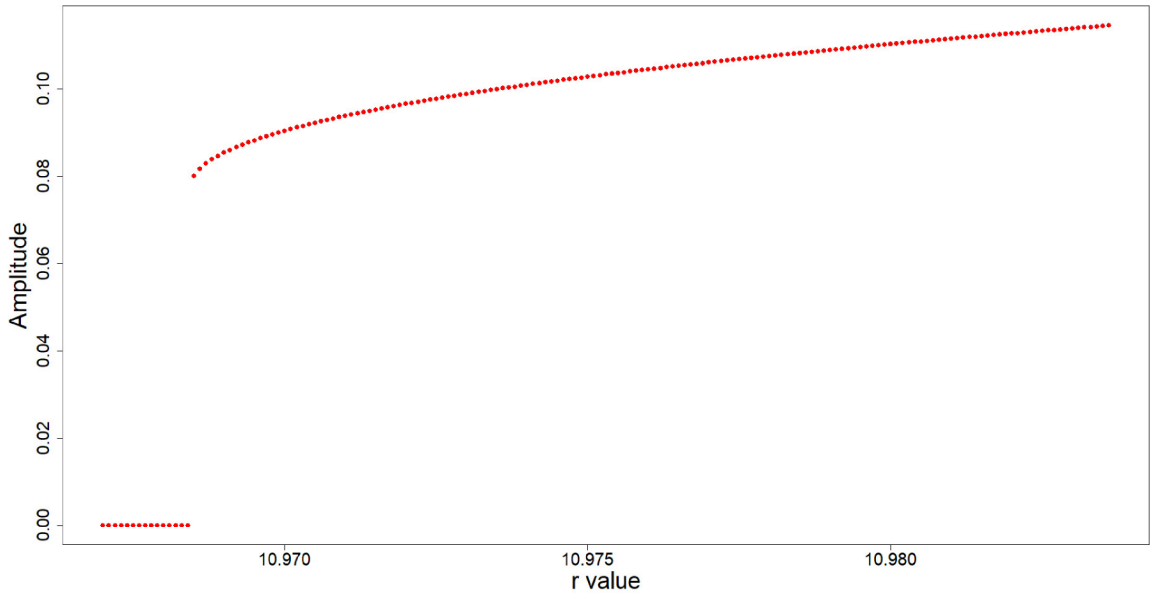

Figure 7.4: A plot of amplitude by r, created by slowly decreasing r, with the initial conditions taken as the limit cycle at the previous r value.

The second method, which produced Figure 7.5, has a different, constant, initial condition for each r. More specifically, for each r value, the initial condition is taken near the equilibrim, as $x(t) = \frac{r-\tilde{\gamma}}{r} - 0.001$ for $t \in [-1, 0]$, and the amplitude for each r is calculated as described in a previous paragraph. In this plot, we see that when starting near the equilibrium value, solutions initially converge to the equilibrium until amplitude suddenly jumps up by $r = 10.9831$, when solitions start converging to the limit cycle, indicating the loss of stability at the nonzero equilibrium. This happens farther to the right of the theoretical value computed by Maple. So, when $r \geq 10.9831$, equation (2.0.1) has a stable limit cycle.

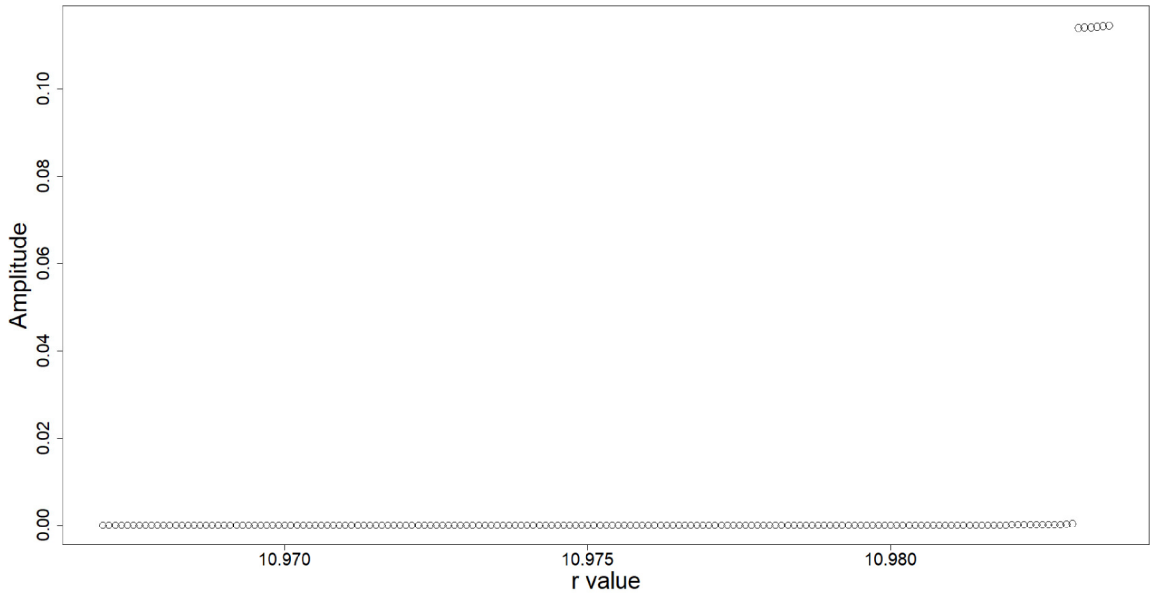

Figure 7.5: A plot of amplitude by r when the initial condition for each r value is taken as $(equilibrium - 0.001)$.

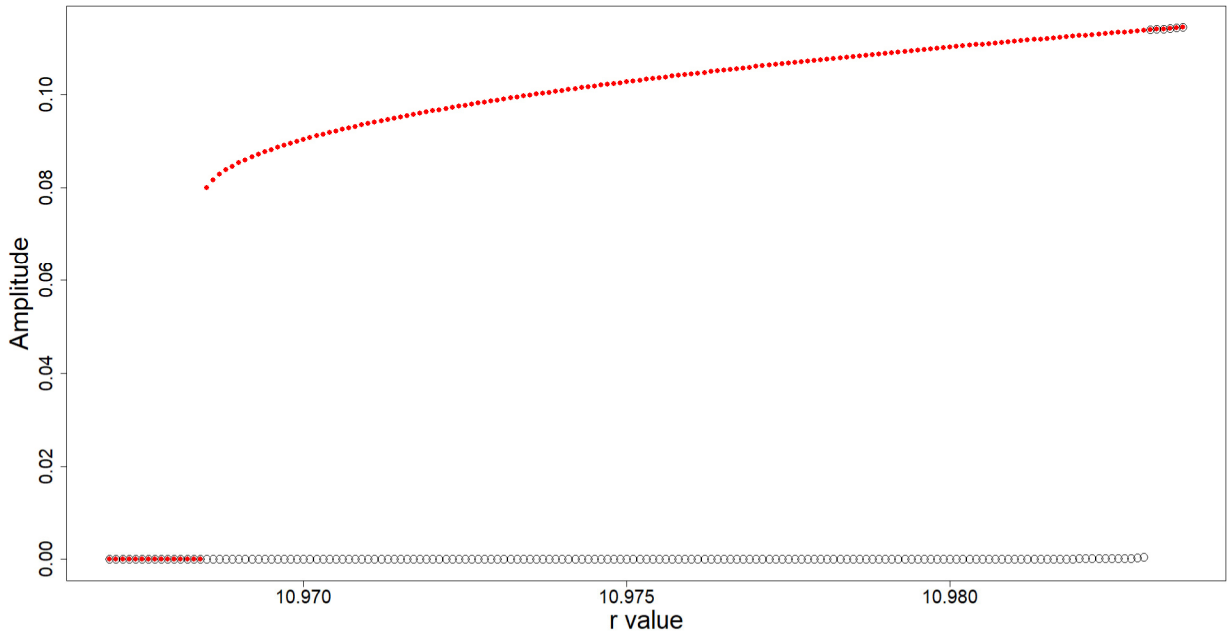

Figure 7.6: A plot of amplitude by r value which combines the previous two plots.

Figure 7.6 combines the information from Figures 7.4 and 7.5 in one plot, showing what appears as the solid blue lines in Figure 6.2. Looking at the red dots, we see

that the point where they drop to zero, corresponds to the point r_1 in Figure 6.2, which in this case is an r value between 10.9684 and 10.9685, so that to the left of this value, we know that all solutions will converge to the stable equilibrium. Looking at the circles, we see that when we start near the equilibrium, and slowly increase r, the solutions will converge to the equilibrium until we pass an r value, between 10.9830 and 10.9831 in this case, which corresponds to r_0 in Figure 6.2, when solutions start converging to the stable, outer limit cycle. After r has passed r_0 we see that even if we then start decreasing it back down, the solutions will continue converging to the stable limit cycle instead of the equilibrium. These jumps that occur, at r_1, from the stable limit cycle to the stable equilibrium, and at r_0, from the stable equilibrium to the stable limit cycle, are characteristic of a phenomenon known as *hysteresis* [14].

The next step is to obtain plots which show the behavior of solutions $x(t)$ by time, for two different values of r.

For Figure 7.7, an r value to the left of the sudden drop in amplitude in Figure 7.4, was chosen. Choosing $r = 10.88$, and the interval for t as $[-1, 300]$, since this is considered a long enough time interval to determine the behaviour of the solutions, and a constant initial condition of $x(t) = 0.6$ for $t \in [-1, 0]$, so that it is not far from the equilibrium of ≈ 0.583383, the plot in Figure 7.7 is produced. In this plot the solutions seem to converge to the equilibrium, therefore having an amplitude of zero and showing a stable equilibrium, as would be expected before a subcritical Hopf bifurcation.

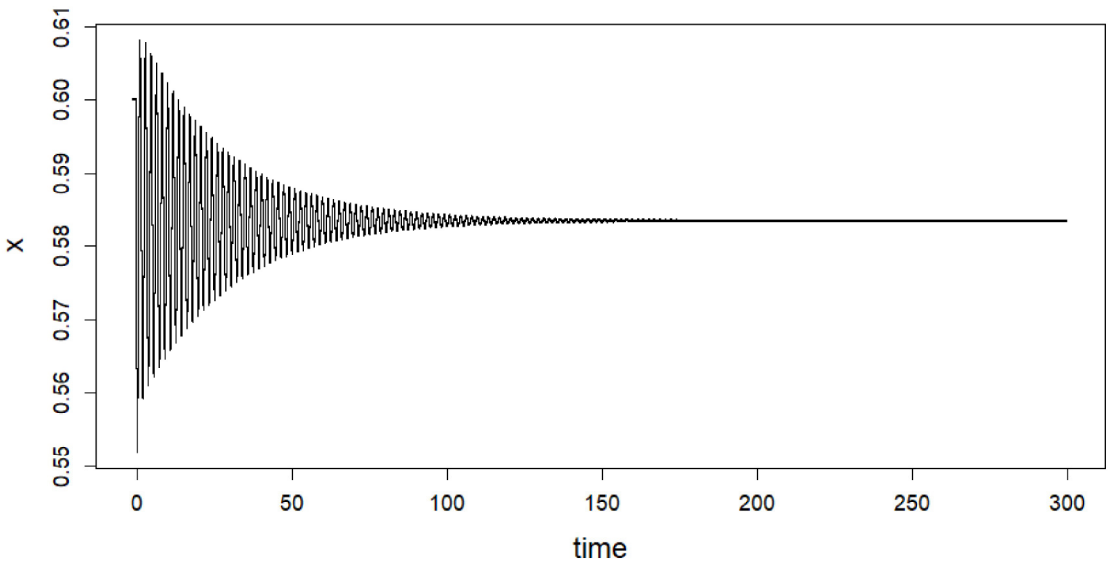

Figure 7.7: A plot of solutions, x, by time, when $r = 10.88$.

Next, we take an r value from Figure 7.6, which can correspond to both a positive amplitude from the red dots, or a zero amplitude shown by the circles. Choosing $r = 10.975$, it will be shown that depending on the initial condition, the solutions $x(t)$ can either converge to the equilibrium or to a stable limit cycle, where the solutions oscillate about the equilibrium with nonzero amplitude. The equilibrium when $\omega = 3.5$ is $\frac{10.975-4.532792698}{10.975} \approx 0.587$. Both plots will be of solutions $x(t)$ by time, from -1 to T, where T is chosen to be large enough to show the long term behavior, and is divided into intervals of the length 0.001 (since $\Delta t = 0.001$ in the Forward Euler method), and x is evaluated at each indexed time. In the first case, the initial condition is taken as $x(t) = 0.55$ when $t \in [-1, 0]$, and in Figure 7.8, is the plot of solutions, $x(t)$, by time from -1 to 500. In this figure, it appears that the solutions are oscillating about the equilibrium, growing in amplitude, until they appear to stabilize, which would suggest they converge to a limit cycle, and the amplitde appears to be just over 0.1, as is expected considering Figure 7.6.

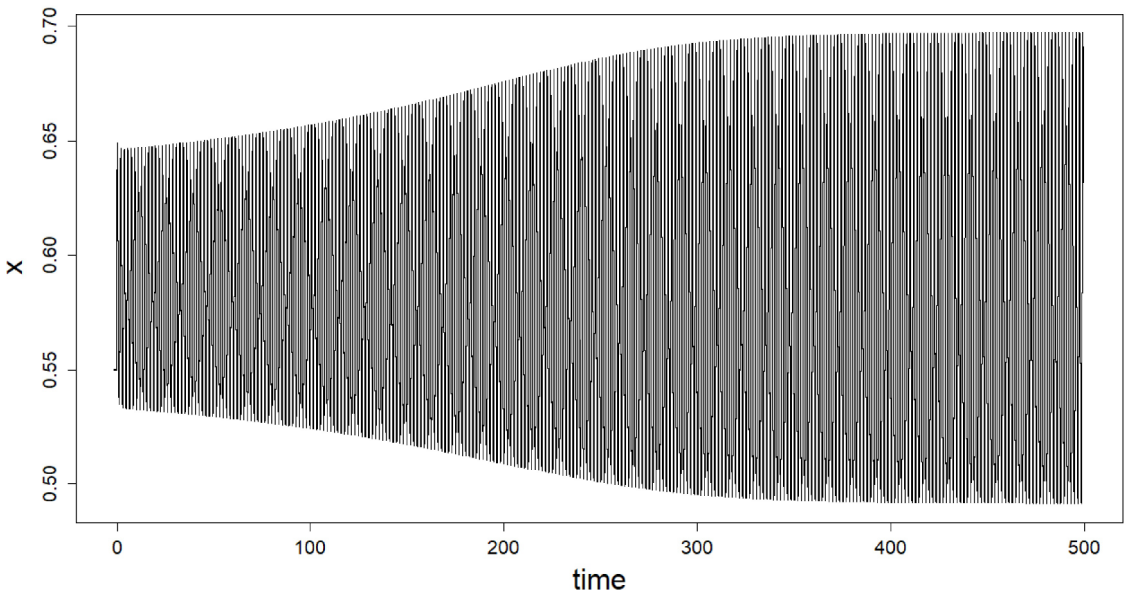

Figure 7.8: A plot of solutions, x, by time, when $r = 10.975$ starting with a constant initial condition of $x(t) = 0.55$ when $t \in [-1, 0]$.

For the second plot an initial condition of $x(t) = 0.6$ for $t \in [-1, 0]$, closer to the equilibrium value, was chosen. It was considered that a longer time interval was needed to determine the behavior of the solutions, so Figure 7.9 shows a plot of $x(t)$ for time from -1 to 2000. From the plot it can be seen that the solutions appear to be oscillating about the equilibrium, with amplitude slowly decreasing, until the

solutions appear to converge to the equilibrium value.

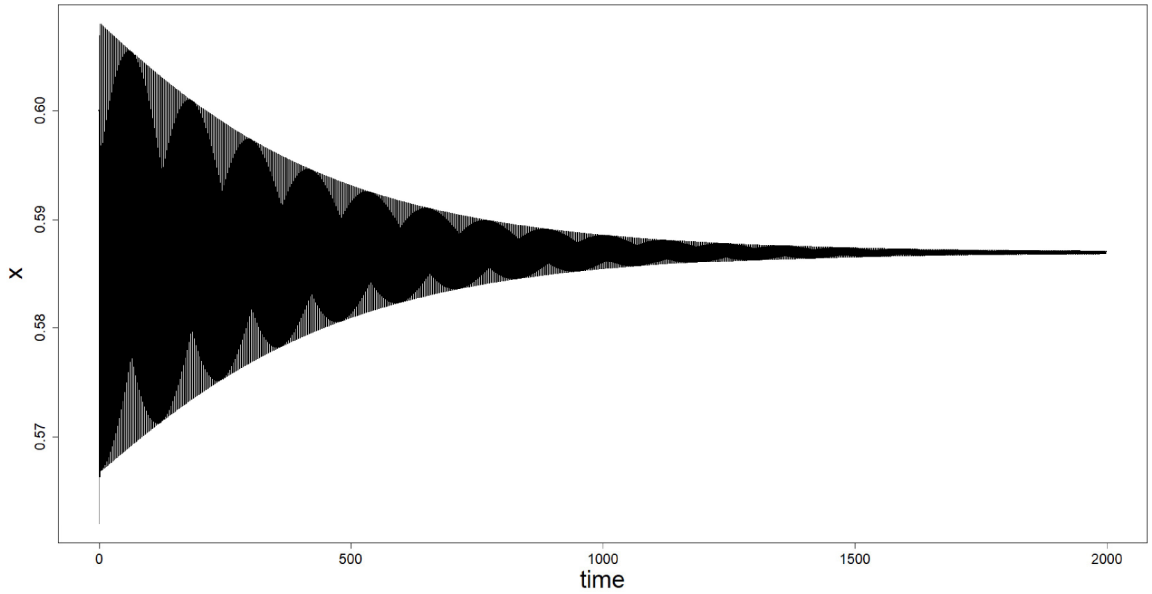

Figure 7.9: A plot of solutions, x, by time, when $r = 10.975$ starting with a constant initial condition of $x(t) = 0.6$ when $t \in [-1, 0]$.

So, when the initial condition is near the equilibrium point the solutions converge to the equilibrium. When the initial condition is a bit farther away, solutions converge to a limit cycle. This dependence of the population level on the initial condition is a result of multi-stability, which referring to Figure 7.6 and the related paragraph that follows it, occurs when r is between r_1 and r_0.

Chapter 8

Conclusion

We have obtained some results that give us a better understanding of the possible behavior of solutions at a Hopf bifurcation of the nonzero equilibrium for the PMC model (1.0.2), which has one delay, and a DDE with two delays (1.0.3), which is a slightly modified version of the PMC model. As variants of the well known logistic equation, they can be used as models for population dynamics, so studying their behavior helps one obtain more information on how a species population could behave. For both cases, the first thing that was done was to non-dimensionalize the models, and obtain a Taylor expansion about the nonzero equilibrium, which for both equations is $y^* = \frac{r-\tilde{\gamma}}{rc}$.

For the PMC model, we expanded on the work done in [16], by obtaining a formula for the first Lyapunov coefficient, K, followed by a theorem and proof that K is always negative or zero $\forall\, \omega$, implying that the Hopf bifurcation is always supercritical when $K \neq 0$. In this proof, we have also shown the use of $A + B\frac{\sin(\omega)}{\omega}$ as a method of finding the sign of a complicated expression involving $\cos(\omega)$ and $\sin(\omega)$. The numerical simulations in Chapter 7, Figures 7.1 to 7.3, for certain parameter values show the behavior expected from a supercritical bifurcation, where we have a stable equilibrium until r is increased past a critical value, r_0. We see that when $r < r_0$ solutions will converge to the stable equilibrium, but when $r > r_0$, the equilibrium looses stability and we have the appearance of a stable limit cycle towards which the solutions start converging to. So for the population of a species, this implies that when the intrinsic growth rate increases past r_0, the population level will no longer converge to the equilibrium but to a stable limit cycle instead, which implies that the population levels will oscillate. However, this is reversible, as decreasing r back below r_0 will return the population level to its equilibrium value [14]. Therefore, for populations following the PMC model, an increase in growth rate past a critical value, considering the other parameters are unchanged, is not so problamatic since it could potentially be reversed.

The main model studied is similar to the PMC model, but has two delays, with

the second delay included for the death rate term. We have shown that the inclusion of that second delay term leads to more complex behavior of the solutions at the Hopf bifurcation for the nonzero equilibrium. We have found a region of stability for the nonzero equilibrium using bounds on r and the characteristic equation at a Hopf bifurcation, after which we find a formula for the first Lyapunov coefficient, K, when $c = 1$ and $\tau = \frac{1}{3}$, for illustrative purposes. We obtain a plot of K by ω and see that K crosses the x-axis, changing sign, which implies that we need to calculate the second Lyapunov coefficient for the cases where $K = 0$ to better understand the behavior of the solutions. After plotting the second Lyapunov coefficient, labelled K_4, we see that there are values of ω where K and K_4 have opposing signs, which can lead to interesting behavior at the Bautin bifurcation.

We chose to look at what happens at $\omega = 3.5$, just before a positive K crosses the x-axis, and $K_4 < 0$, which implies that at the Bautin bifurcation the Hopf bifurcation will turn from subcritical to supercritical, as illustrated in Figure 6.2. This behavior can also be seen in the numerical simulations in Figures 7.4 to 7.9 of Chapter 7, where we see a phenomenon called *hysteresis*, characterized by a jump in solutions from one stable equilibrium to another [14]. For example, this can be seen in Figure 7.6, occuring at an r value between 10.9830 and 10.9831, corresponding to r_0 in Figure 6.2, at which the equilibrium looses stability and solutions suddenly jump up to the stable limit cycle, after which even if we decrease r back down to try to bring the solutions back to the equilibrium, the solutions will continue converging to the stable limit cycle. For a species population this implies that if the intrinsic growth rate is increased past a certain critical value r_0, population levels will start oscillating, and decreasing r back below r_0 will not bring population levels back down to their equilibrium value. So, while for the PMC model we can decrease r back below r_0 to return the solutions to the equilibrium, this will not work if we include a second delay term in the PMC model, in which case the loss of stability at the equilibrium is more problamatic. In Figure 7.6 we also see multi-stability when the growth rate, r, is between r_1 and r_0, so that for r in this interval, the population level depends on the initial condition, as shown with Figures 7.8 and 7.9. This is important because it makes it harder for someone to predict the population level of a species for which the population level can be modelled by equation (1.0.3). One would need to know the initial condition, and even then, a small difference in the initial condition can lead to a different outcome: equilibrium versus oscillating population levels.

Therefore, if the population of a species can be modelled using one of these equations, we have given some information on possible behavior that the population could exhibit. Some situations that can cause an increase in r are a lack of predators, abundance of food or more optimal conditions for offspring survival.

One example could be the case of invasive species. When brought to new environments they most likely lack natural predators, and if the environment is favorable for their survival there is the possibility that their growth rate increases compared to

that in their native habitat, where they are more likely to exist at equilibrium levels. If this growth rate increases past a certain critical value, population levels can start oscillating, at potentially higher levels which can end up having a negative impact on the ecosystem they have migrated to, affecting other plant or animal species, and there is no returning to equilibrium levels.

Another example could involve mosquito populations. With the weather becoming less predicatable as a result of climate change, some regions of the world might see increased rainfall or warmer weather than usual, conditions which are favorable to mosquito populations, and which could lead to an increase in their growth rate. If mosquito populations follow a population model like (1.0.3), and their growth rate r increases past a certain critical value, their population levels may no longer converge to their previous equilibrium levels but jump to the stable limit cycle and start oscillating. After this, even if something causes a decrease in their growth rate, like perhaps a period of drought, their population levels will not return to their equilibrium values. Oscillating mosquito populations could imply larger mosquito populations, which is unpleasant for humans, other animals, and potentially dangerous as they can carry diseases.

While here we have focused on studying the behavior of equation (1.0.3) at a Hopf bifurcation, it could be of interest to study the behavior of this equation at other bifurcation types, like a cusp bifurcation or a Bogdanov-Takens bifurcation. One can look at whether they could occur, and if so, under what conditions, and analyse the resulting behavior. Continuing on from the work done here, another topic of future research could be a study of the behavior of a generalized version of (1.0.3), of the form

$$\dot{x}(t) = r(a_1x(t) + a_2x(t-\tau_1))(b_1 - b_2x(t) - b_3x(t-\tau_1)) - \gamma x(t-\tau_2), \qquad (8.0.1)$$

where the presence of $x(t)$ alongside $x(t-\tau_1)$ imply a one-species population model where both immature and adult members of the species are competing for resources. The analysis of a Hopf bifurcation is expected to be much more complicated and lengthier.

As was mentioned in the introduction, many authors have looked at predator-prey models which incorporate delays, looking at equilibrium stability and properties of the Hopf bifurcation. With this in mind, it might be interesting to do such an analysis for a predator-prey model where either prey or predator is harvested, and to use equation (1.0.3) for the harvested species. Of course, in this case equation (1.0.3) would have to be modified a bit, by including an interaction term.

Appendix A

Maple code

The following code was used to find the first Lyapunov coefficient for the PMC model and the plot, shown in Chapter 4. The output is not shown. The code used for finding the first Lyapunov coefficient for the main model (1.0.3) is similar.

```
with(LinearAlgebra)

expand(Multiply(x1*exp(-I*omega) + x2*exp(omega*I) + x3 + x4*exp(-2*I*omega), x1*exp(-I*omega) + x2*exp(omega*I) + x3 + x4*exp(-2*I*omega)))

T1 := -gam - omega*I;

T2 := gam - r;

T3 := (((gam^2 + 2*I*omega*gam - omega^2) - 2*gam^2) + r*gam)/(2*gam - r);

EC := (-4*r^2*c^2*exp(-I*omega)/T2 + 2*r^2*c^2*exp(-2*I*omega)*exp(-I*omega)/(2*I*omega - T3))/(1 - T1);

K := evalc(Re(EC));

A := gam;

b := -2*gam + r;

EQ := omega*I + A + b*exp(-I*omega);

EQr := evalc(Re(EQ));

EQi := evalc(Im(EQ));

solve(EQr, r);

r := %;

EQi;

solve(EQi, gam)

gam := %

K

simplify(%, 'trig')

c := 1

with(plots)

plot(K, omega = 0.001 .. 9, -4 .. 2, labels = ["omega;", "K"], labelfont = ["Times", 17])
```

This following section of code, written by my supervisor, Dr. Victor LeBlanc, was used to obtain a formula for the second Lyapunov coefficient for the main model, equation (1.0.3). Again the output is not included.

```
c := 1;
tau := 1/3;
z := h04*wb^4 + h13*w*wb^3 + h22*w^2*wb^2 + h31*w^3*wb + h40*w^4 + h03*wb^3 + h12*w*wb^2 + h21*w^2*wb + h30*w^3 + h02*wb^2 + h11*w*wb + h20*w^2 + w;
zb := h04b*w^4 + h13b*w^3*wb + h22b*w^2*wb^2 + h31b*w*wb^3 + h40b*wb^4 + h03b*w^3 + h12b*w^2*wb + h21b*w*wb^2 + h30b*wb^3 + h02b*w^2 + h11b*w*wb +
      h20b*wb^2 + wb;


y := theta -> g20(theta)*w^2 + g11(theta)*w*wb + g02(theta)*wb^2 + g30(theta)*w^3 + g21(theta)*w^2*wb + g12(theta)*w*wb^2 + g03(theta)*wb^3 + g40(theta)*w^4 +
      g31(theta)*w^3*wb + g22(theta)*w^2*wb^2 + g13(theta)*w*wb^3 + g04(theta)*wb^4

F1 := omega*z*I - (beta1 + beta2*I)*c*r*(exp(-I*omega)*z + exp(omega*I)*zb + y(-1))^2;
F1b := -omega*zb*I - (beta1 - beta2*I)*c*r*(exp(-I*omega)*z + exp(omega*I)*zb + y(-1))^2;
with(linalg)
A := array([[diff(z, w), diff(z, wb)], [diff(zb, w), diff(zb, wb)]])
IA := inverse(A);
G := F1*IA[1, 1] + F1b*IA[1, 2];
Gb := F1*IA[2, 1] + F1b*IA[2, 2];
w := eps*W;
wb := eps*Wb;

series(G, eps, 6);
convert(%, polynom, eps);
G := collect(%, {W, Wb}, distributed);
series(Gb, eps, 6);
convert(%, polynom, eps);
Gb := collect(%, {W, Wb}, distributed);
eps := 1;

w := 'w';
wb := 'wb';
W := w;
Wb := wb;

G;
G := %;
Gb;
Gb := %;
eps := 'eps';

H := G*diff(y(theta), w) + Gb*diff(y(theta), wb) - diff(y(theta), theta) - ((beta1 + beta2*I)*exp(omega*theta*I)
     + (beta1 - beta2*I)*exp(-I*omega*theta))*c*r*(exp(-I*omega)*z + exp(omega*I)*zb + y(-1))^2;

W := 'W';
Wb := 'Wb';
w := eps*W;
wb := eps*Wb;

series(H, eps, 6);
convert(%, polynom, eps);
H := %;
w := 'w';
wb := 'wb';

W := w;
Wb := wb;
eps := 1;

H;
H := collect(%, {w, wb}, distributed);
L1 := expand(coeff(coeff(G, w, 2), wb, 1));
L2 := expand(coeff(coeff(G, w, 3), wb, 2));

X0P := -D(y)(0) - c*r*(exp(-I*omega)*z + exp(omega*I)*zb + y(-1))^2 - gam*y(-tau) + (2*gam - r)*y(-1);
W := 'W';
Wb := 'Wb';

eps := 'eps'
w := eps*W;
wb := eps*Wb;

series(X0P, eps, 6);
convert(%, polynom, eps);
X0P := %;
w := 'w';
wb := 'wb';
eps := 1;
W := w;
Wb := wb;

X0P := collect(X0P, {w, wb}, distributed);
solve({coeff(coeff(G, w, 0), wb, 2), coeff(coeff(G, w, 1), wb, 1), coeff(coeff(G, w, 2), wb, 0), coeff(coeff(Gb, w, 0), wb, 2),
        coeff(coeff(Gb, w, 1), wb, 1), coeff(coeff(Gb, w, 2), wb, 0)}, {h02, h02b, h11, h11b, h20, h20b});

assign(%);
```

```
P20 := dsolve(coeff(coeff(H, w, 2), wb, 0), g20(theta));
g20 := unapply(rhs(P20), theta)
solve(coeff(coeff(X0P, w, 2), wb, 0), _C1)
_C1 := %

P11 := dsolve(coeff(coeff(H, w, 1), wb, 1), g11(theta))
g11 := unapply(rhs(%), theta)

solve(coeff(coeff(X0P, w, 1), wb, 1), _C2);
_C2 := %;

P02 := dsolve(coeff(coeff(H, w, 0), wb, 2), g02(theta))
g02 := unapply(rhs(%), theta)
solve(coeff(coeff(X0P, w, 0), wb, 2), _C3)
_C3 := %

solve({coeff(coeff(G, w, 0), wb, 3), coeff(coeff(G, w, 1), wb, 2), coeff(coeff(G, w, 3), wb, 0), coeff(coeff(Gb, w, 0), wb, 3), coeff(coeff(Gb, w, 2), wb, 1),
        coeff(coeff(Gb, w, 3), wb, 0)}, {h03, h03b, h12, h12b, h30, h30b});
assign(%);
h21 := 0;
h21b := 0;

P30 := dsolve(coeff(coeff(H, w, 3), wb, 0), g30(theta));
g30 := unapply(rhs(%), theta);
solve(coeff(coeff(X0P, w, 3), wb, 0), _C4);
_C4 := %;
P21 := dsolve(coeff(coeff(H, w, 2), wb, 1), g21(theta));
g21 := unapply(rhs(%), theta);

P12 := dsolve(coeff(coeff(H, w, 1), wb, 2), g12(theta));
g12 := unapply(rhs(%), theta);

P03 := dsolve(coeff(coeff(H, w, 0), wb, 3), g03(theta));
g03 := unapply(rhs(%), theta);
solve(coeff(coeff(X0P, w, 0), wb, 3), _C5);
_C5 := %;

solve({coeff(coeff(G, w, 0), wb, 4), coeff(coeff(G, w, 1), wb, 3), coeff(coeff(G, w, 2), wb, 2), coeff(coeff(G, w, 3), wb, 1), coeff(coeff(G, w, 4), wb, 0),
        coeff(coeff(Gb, w, 0), wb, 4), coeff(coeff(Gb, w, 1), wb, 3), coeff(coeff(Gb, w, 2), wb, 2), coeff(coeff(Gb, w, 3), wb, 1),
        coeff(coeff(Gb, w, 4), wb, 0)}, {h04, h04b, h13, h13b, h22, h22b, h31, h31b, h40, h40b});
assign(%);

LC := expand(evalc(Re(coeff(coeff(G, w, 2), wb, 1))));

evalf(coeff(coeff(H, w, 4), wb, 0));
expand(%);
QQ40 := %;
dsolve(QQ40, g40(theta));
g40 := unapply(rhs(%), theta);
C40 := collect(expand(coeff(coeff(X0P, w, 4), wb, 0)), _C6);
_C6 := -coeff(C40, _C6, 0)/coeff(C40, _C6, 1);

evalf(coeff(coeff(H, w, 3), wb, 1));
expand(%);
QQ31 := %;
dsolve(QQ31, g31(theta));
g31 := unapply(rhs(%), theta);
C31 := collect(expand(coeff(coeff(X0P, w, 3), wb, 1)), _C7);
_C7 := -coeff(C31, _C7, 0)/coeff(C31, _C7, 1);

evalf(coeff(coeff(H, w, 2), wb, 2));
expand(%);
Q22 := %;
dsolve(Q22, g22(theta));

g22 := unapply(rhs(%), theta);

C22 := collect(expand(coeff(coeff(X0P, w, 2), wb, 2)), _C8);
_C8 := -coeff(C22, _C8, 0)/coeff(C22, _C8, 1);

g13 := theta -> conjugate(g31(theta));
g04 := theta -> conjugate(g40(theta));

L1 := expand(L1);
L2 := expand(L2);
save L1, L2, "Lyapunovcoefficients.m";
```

Next, the following code was used to calculate 100 points for a plot of K and K_4 for $\omega \in [1, 5]$ using the formulas obtained with previous code.

```
read "c:/Teza/Maple/Lyapunovcoefficients.m";
L1;
with(LinearAlgebra)
```

```
with(plots)
beta1 := evalc(Re(1/(1 + (2*gam - r)*exp(-I*omega) - gam*tau*exp(-I*omega*tau))))
beta2 := evalc(Im(1/(1 + (2*gam - r)*exp(-I*omega) - gam*tau*exp(-I*omega*tau))))

EQ := omega*I - (2*gam - r)*exp(-I*omega) + gam*exp(-I*omega*tau);
EQr := evalc(Re(EQ));
EQi := evalc(Im(EQ));
solve(EQr, r);
r := %;
EQi;
solve(EQi, gam);
gam := %;
tau := 1/3;

plot(evalc(Re(L1)), omega = 1 .. 6, -100 .. 300);

omega = 1 .. 5;
data := [];

for i to 100 do
    omega[i] := 1 + (4*i)/100;
    omega := evalf(omega[i]);
    K1[i] = evalf(evalc(Re(L1)));
    data := [op(data), [omega, evalf(evalc(Re(L1)))]];
end do;

save data, "L1values.m";
plot(data);

omega = 1 .. 5;
data2 := [];

for i to 100 do
    omega[i] := 1 + (4*i)/100;
    omega := evalf(omega[i]);
    data2 := [op(data2), [omega, evalf(evalc(Re(L2)))]];
end do;
save data, "L2values.m";
plot(data2);
```

The following code was used to scale the values of K_4, and to obtain the plot where K appears alongside K_4 in Chapter 6.

```
read "c:/Teza/Maple/L1values.m";
data;
with(plots)
A := plot([data], color = blue, thickness = 3)
read "c:/Teza/Maple/L2values.m";
data2;

omega = 1 .. 5;
data3 := [];

for i to 100 do
    omega[i] := 1 + (4*i)/100;
    omega := evalf(omega[i]);
    t[i] := data2[i, 2]/1000;
    t := evalf(t[i]);
    data3 := [op(data3), [omega, t]];
end do;

B2 := plot(data3, color = red, thickness = 3)

display(A, B2, labels = ["omega;", ""], title = "First and Second Lyapunov Coefficients ", titlefont = ["ROMAN", 22, bold], labelfont = ["ROMAN", 20, bold])
```

Appendix B

R code

The following code was used to obtain the plot of amplitude by r for the PMC model, for r values from 4.7 to 5.2.

```
T = 100
t = 0.001
gam=1.228180394
c1=1
c2=1
time <- seq(from = -1, to = T, by = t)
x <- integer(length(time)) #Setting null array to be same length as time array

for(i in 1:1001) {
  x[i] = 0.75
}

r_set <- seq(from = 4.7, to = 5.2, by = 0.01)

amp_set <- integer(length(r_set))
amp_loop <- integer(1000)
diff_amp = 1000

for (f in 1:length(r_set)){

  r = r_set[f]
  ind = 0
  diff_amp = 1000
  ind = 0

  while (diff_amp > 0.00001){

    for (i in 1:100000){
      x[1001 + i] = x[1001+i-1] + t*(r*x[1001+i-1000]*(c1-c2*x[1001 +i-1000])- gam*x[1001 + i - 1])
    } #Creating a loop for DDE.

    x[1:1001] = x[which(time == 99):which(time == 100)]   ##resets initial condition.

    print(r)
    amp = (max(x) - min(x))/2
    amp_set[f] = amp
    print(amp)

    ind = ind + 1
    amp_loop[ind] = amp

    if (ind >= 2){
      diff_amp = abs(amp_loop[ind] - amp_loop[ind-1])
    }
  }
}
par(mar = c(4.2, 5.2, 0.5, 0.5))
plot(r_set, amp_set, cex=1.5, pch= 19, xlab = "r value", ylab = "Amplitude", cex.lab= 2.5, cex.axis=1.8)
```

The following code was used to obtain the plots of $x(t)$ by time for the PMC model. This code is for the case where $r = 4.7$ with a constant initial condition of

$x(t) = 0.7$ for $t \in [-1, 0]$. The same code was used for the case when $r = 5$, with the necessary adjustments.

```
T = 200
t = 0.001
gam=1.228180394
r=4.7
c1=1
c2=1

Eqm = (r-gam)/r
Eqm

time <- seq(from = -1, to = T, by = t)

x <- integer(length(time)) #Setting null array to be the same length as time array

for(i in 1:1001) {
  x[i] = 0.7
}

for (i in 1:200000){
  x[1001 + i] = x[1001+i-1] + t*(r*x[1001+i-1000]*(c1-c2*x[1001 +i-1000])- gam*x[1001 + i - 1])
}
plot(time, x, cex=0.2, cex.lab= 1.8, cex.axis=1.4)
```

The following code was used to obtain the first three plots of amplitude by r for the main model, equation (1.0.3). This first part is used to obtain values of $x(t)$ on the limit cycle when $r = 10.990$.

```
T = 100
t = 0.001
gam=4.532792698
r=10.990
c1=1
c2=1

time <- seq(from = -1, to = T, by = t)  #Set time array.

x <- integer(length(time)) #Setting null array to be the same length as time array

for(i in 1:1001) {
  x[i] = 0.6
} #Create for loop for time [-1, 0].

for (d in 1:100){

  for (i in 1:100000){
    x[1001 + i] = x[1001+i-1] + t*(r*x[1001+i-1000]*(c1-c2*x[1001 +i-1000])- gam*x[round(1001 + i - (1000/3), digits = 0)])
  }#Creating a loop for DDE.

  x[1:1001] = x[which(time == 99):which(time == 100)]   ##resets initial condition.

}
plot(time, x, cex=0.2)
```

Now, from this last plot, we use the values of $x(t)$ on the interval $t \in [99, 100]$ so that we can start near the limit cycle to obtain the first plot of amplitude by r in Chapter 7 for (1.0.3).

```
r_set <- seq(from = 10.9836, to = 10.967, by = -0.0001)

amp_set <- integer(length(r_set))
amp_loop <- integer(1000)
diff_amp = 1000

x[1:1001] = x[which(time == 99):which(time == 100)]   ##resets initial condition.

for (f in 1:length(r_set)){

  r = r_set[f]
  ind = 0
  diff_amp = 1000
  ind = 0
```

```
  while (diff_amp > 0.00001){

    for (i in 1:100000){
      x[1001 + i] = x[1001+i-1] + t*(r*x[1001+i-1000]*(c1-c2*x[1001 +i-1000])- gam*x[round(1001 + i - (1000/3), digits = 0)])
    }

    x[1:1001] = x[which(time == 99):which(time == 100)]   ##resets initial condition.

    print(r)
    amp = (max(x) - min(x))/2
    amp_set[f] = amp
    print(amp)

    ind = ind + 1
    amp_loop[ind] = amp

    if (ind >= 2){
      diff_amp = abs(amp_loop[ind] - amp_loop[ind-1])
    }
  }
}
par(mar = c(4.2, 5.2, 0.5, 0.5))
plot(r_set, amp_set, cex=1.1, col="red", xlab = "r value", ylab = "Amplitude", cex.lab= 2.5, cex.axis=1.8, pch=16)
```

This code takes, for each r value, the initial condition to be the *equilibrium* - 0.001 for $t \in [-1, 0]$. The last line of code combines these last two plots.

```
T = 100
t = 0.001
gam=4.532792698
c1=1
c2=1

r_set <- seq(from = 10.9836, to = 10.967, by = -0.0001)

amp_set2 <- integer(length(r_set))
amp_loop <- integer(1000)
diff_amp = 1000

for (f in 1:length(r_set)){

  r = r_set[f]

  Eqm = (r-gam)/r

  for(i in 1:1001) {
    x[i] = Eqm - 0.001
  }

  ind = 0
  diff_amp = 1000
  ind = 0

  while (diff_amp > 0.000001){

    for (i in 1:100000){
      x[1001 + i] = x[1001+i-1] + t*(r*x[1001+i-1000]*(c1-c2*x[1001 +i-1000])- gam*x[round(1001 + i - (1000/3), digits = 0)])
    }

    x[1:1001] = x[which(time == 99):which(time == 100)]   ##resets initial condition.

    print(r)
    amp = (max(x) - min(x))/2
    amp_set2[f] = amp
    print(amp)

    ind = ind + 1
    amp_loop[ind] = amp

    if (ind >= 2){
      diff_amp = abs(amp_loop[ind] - amp_loop[ind-1])
    }
  }
}
par(mar = c(4.2, 5.2, 0.5, 0.5))
plot(r_set, amp_set2, cex=1.5, xlab = "r value", ylab = "Amplitude", cex.lab= 2.5, cex.axis=1.8, pch = 16)
points(r_set, amp_set, cex=1.1, pch=16, col="red")
```

This is one example of the code used to obtain the last three plots, of $x(t)$ by time, for equation (1.0.3). This code corresponds to the case that $r = 10.975$ with

an initial condition of $x(t) = 0.55$ for $t \in [-1, 0]$. The other two are found similary, making the necessary adjustments.

```
T = 500
t = 0.001
gam=4.532792698
r=10.975
c1=1
c2=1

Eqm = (r-gam)/r
Eqm

time <- seq(from = -1, to = T, by = t)

x <- integer(length(time))

for(i in 1:1001) {
  x[i] = 0.55
}

for (i in 1:500000){
  x[1001 + i] = x[1001+i-1] + t*(r*x[1001+i-1000]*(c1-c2*x[1001 +i-1000])- gam*x[round(1001 + i - (1000/3), digits = 0)])
}

plot(time, x, cex=0.01, cex.lab= 2, cex.axis=1.3)
```

Bibliography

[1] W. G. Aiello and H. I. Freedman. A time-delay model of single-species growth with stage structure. *Mathematical Biosciences*, 101:139–153, 1990.

[2] N. Bairagi and D. Jana. On the stability and Hopf bifurcation of a delay-induced predator-prey system with habitat complexity. *Applied Mathematical Modelling*, 35:3255–3267, 2011.

[3] R. D. Braddock and P. Van Den Driessche. On a two lag differential delay equation. *J. Austral. Math Soc*, 24:292–317, 1983.

[4] F. Brauer. Stability of some population models with delay. *Mathematical Biosciences*, 33:345–358, 1977.

[5] C. Celik. The stability and Hopf bifurcation for a predator-prey system with time delay. *Chaos, Solitons and Fractals*, 37:87–99, 2008.

[6] T. Faria and L. T. Magalhães. Normal forms for retarded functional differential equations and applications to Bogdanov-Takens singularity. *Journal of Differential Equations*, 122:201–224, 1995.

[7] T. Faria and L. T. Magalhães. Normal forms for retarded functional differential equations with parameters and applications to Hopf bifurcation. *Journal of Differential Equations*, 122:181–200, 1995.

[8] N. H. Gazi. Dynamics of populations in fish farm: Analysis of stability and direction of Hopf-bifurcating periodic oscillation. *Applied Mathematical Modelling*, 36:2118–2127, 2012.

[9] J. K. Hale and S. M. Verduyn Lunel. *Introduction to Functional Differential Equations*. Springer-Verlag, New York, 1993.

[10] B.D. Hassard, N.D. Kazarinoff, and Y.H. Wan. *Theory and Applications of Hopf Bifurcation*. Cambridge University Press, Cambridge, 1981.

[11] G. Huang, A. Liu, and U. Forys. Global stability analysis of some nonlinear delay differential equations in population dynamics. *Journal of Nonlinear Science*, 26:27–41, 2016.

[12] T. K. Kar. Selective harvesting in a prey-predator fishery with time delay. *Mathematical and Computer Modelling*, 38:449–458, 2003.

[13] T. K. Kar and U. K. Pahari. Modelling and analysis of a prey-predator system with stage-structure and harvesting. *Nonlinear Analysis: Real World Applications*, 8:601–609, 2007.

[14] Y. A. Kuznetsov. *Elements of Applied Bifurcation Theory.* Springer, New York, 2004.

[15] X. Li, S. Ruan, and J. Wei. Stability and bifurcation in delay-differential equations with two delays. *Journal of Mathematical Analysis and Applications*, 236:254–280, 1999.

[16] S. Manjunath, A. Podapati, and G. Raina. Stability, convergence, limit cycles and chaos in some models of population dynamics. *Nonlinear Dynamics*, 87:2577–2595, 2017.

[17] J. D. Murray. *Mathematical Biology.* Springer, 1993.

[18] M. Peng, Z. Zhang, and X. Wang. Hybrid control of Hopf bifurcation in a Lotka-Volterra predator-prey model with two delays. *Advances in Difference Equations*, 2017:1–20, 2017.

[19] J. F. Perez, C. P. Malta, and F. A. B. Coutinho. Qualitative analysis of oscillations in isolated populations of flies. *Journal of Theoretical Biology*, 71:505–514, 1978.

[20] L. Perko. *Differential Equations and Dynamical Systems.* Springer, New York, 2001.

[21] M. Senthilkumaran and C. Gunasundari. Stability and Hopf bifurcation in a delayed predator-prey system with parental care for predators. *Journal of Mathematical and Computational Science*, 7:495–521, 2017.

[22] Y. Song, M. Han, and Y. Peng. Stability and Hopf bifurcations in a competitive Lotka-Volterra system with two delays. *Chaos, Solitons and Fractals*, 22:1139–1148, 2004.

[23] Y. Song, W. Xiao, and X. Qi. Stability and Hopf bifurcation of a predator-prey model with stage structure and time delay for the prey. *Nonlinear Dynamics*, 83:1409–1418, 2016.

[24] S. Wiggins. *Introduction to Applied Nonlinear Dynamical Systems and Chaos*. Springer-Verlag, New York, 1990.

[25] Y. Xue and X. Wang. Stability and local Hopf bifurcation for a predator-prey model with delay. *Discrete Dynamics in Nature and Society*, 2012(1-17), 2012.

[26] B. Zheng, M. Tang, and J. Yu. Modelling Wolbachia spread in mosquitoes through delay differential equations. *SIAM Journal on Applied Mathematics*, 74:743–770, 2014.